Summer 8-2013

Biophysical Understanding of Novel Synthetic AMYLOID-β (Aβ) Prions in Alzheimer's Disease

Amit Kumar
University of Southern Mississippi

The University of Southern Mississippi

BIOPHYSICAL UNDERSTANDING OF NOVEL SYNTHETIC AMYLOID-β (Aβ) PRIONS IN ALZHEIMER`S DISEASE.

by

Amit Kumar

Abstract of a Dissertation
Submitted to the Graduate School
of The University of Southern Mississippi
in Partial Fulfillment of the Requirements
for the Degree of Doctor of Philosophy

August 2013

ABSTRACT

BIOPHYSICAL UNDERSTANDING OF NOVEL SYNTHETIC

AMYLOID-β (Aβ) PRIONS IN ALZHEIMER`S DISEASE.

by Amit Kumar

August 2013

Oligomers of amyloid-β (Aβ) peptide are the primary toxic agents that play a pivotal role in the pathogenesis of Alzheimer's disease (AD). Oligomers are the intermediates formed during the Aβ aggregation process leading up to insoluble fibrils. It is important to know that oligomers can also be formed via pathways that do not lead to fibril formation. Such 'off-pathway' oligomers would have significantly longer half-lives than the 'on-pathway' ones, which may result in prolonged toxicity to neuronal cells. Furthermore, neither the mechanism of neurotoxicity nor the potential mechanisms of propagation and proliferation to neighboring cells are well understood. Moreover, recent *in vivo* studies on transgenic animal models have implicated a prion-like mechanism involved in the propagation of toxic oligomeric seeds. Interfaces generated by lipids, fatty acids and other surfactants are well known to affect Aβ aggregation, especially in inducing alternate pathways. In this study, the effect of saturated non-esterified fatty acids (NEFAs) on the rate of Aβ aggregation was studied. We have observed that NEFAs were able to induce an alternate pathway of aggregation, which was depended on NEFA concentrations. More importantly, in a narrow concentration range, NEFAs induced the formation of 12-18mers (Large Fatty Acid-derived Oligomers; LFAOs), which were isolable by size exclusion chromatography (SEC). We discovered that LFAOs can behave like prions, undergoing self-propagation, by quantitatively converting

monomeric Aβ into toxic LFAO assemblies in a template-assisted manner. We further analyzed the prion-like behavior of LFAOs by the 'protein misfolding via cyclic amplification' (PMCA) assay, as was done for prions. Together, our findings indicate that LFAOs are unique Aβ prions and support the developing hypothesis that a common, prion-type mechanism of infectivity could be an underlying conserved mechanism among many neurodegenerative diseases.

The University of Southern Mississippi

BIOPHYSICAL UNDERSTANDING OF NOVEL SYNTHETIC AMYLOID-β (Aβ) PRIONS IN ALZHEIMER`S DISEASE.

by

Amit Kumar

A Dissertation
Submitted to the Graduate School
of The University of Southern Mississippi
in Partial Fulfillment of the Requirements
for the Degree of Doctor of Philosophy

Approved:

Vijay Rangachari
_____
Director

Gordon Cannon
_____

Douglas Masterson
_____

Robert Bateman
_____

Sandra Leal
_____

Susan A. Siltanen
_____
Dean of the Graduate School

August 2013

DEDICATION

I would like to dedicate this dissertation to my father Shri. Ram Narain Singh, my mother Shrimati. Rajkumari, my brothers Anand and Rakesh, my sisters in law Maumita and Sunita, my sister Premlata (Didiya), and my brother in law Akhileshwar Singh for their endless love, blessing and support throughout my career, and especially to my nephew Ashwin and nieces Akash, Rani and Gudiya for making me smile all the time.

ACKNOWLEDGMENTS

Firstly, I would like to thank my graduate mentor, Dr. Vijay Rangachari, for teaching me the fundamentals of research, guiding and motivating me all the time to give my level best and, most importantly, being patient with me.

I would like to thank my committee members, Drs. Gordon Cannon, Douglas Masterson, Robert Bateman and Sandra Leal, for their support, advice, and guidance throughout my PhD career. I would also like to thank my past and current lab members, especially Gaurav, Rebekah and Matthew for their friendship, support and happy times, and also for making me do all their work.

I would also like to thank some of my very dear friends especially, Saurabh, Deepak, Mayank (monu), Sarthak, Dr. Ankur Jain, Rahul (Spity), Manoj, Mridu, Anirban, Souvik, Dhritiman, Adhiraj, Tejal, Kalyani, Dr. Srinivas Konda, Dr. Sunil Pusarla, Dr. Balaraj Menon, Dr. Avijit Biswas, Min Bahadur, Sadhna, Divya, Kavita, Shekhar, Rajni, Nabanita, Sudeshna, Natasha (Nattu), Sonal and Chandrani for their unconditional friendship, beautiful memories and support.

I would also like to thank our collaborators Dr. Sarah Morgan, Dr. John Correia, Dr. Ewa Bienkiewicz, Dr. Peter Fajer, Dr. Likai Song, and their lab members, especially Lea Pasley and Daniel Lyon.

I would also like to thank Dr. Heinhorst, Ms. Sharon King, Ms. Tina Masterson and Martha for their help. I would also like to thank the American Heart Association, USM Department of Chemistry and Biochemistry and USM Graduate School for the funding and support.

TABLE OF CONTENTS

LIST OF ILLUSTRATIONS

Figure

LIST OF ABBREVIATIONS

AD	Alzheimer's disease
Aβ	Amyloid-β
APP	Amyloid Precursor Protein
APF	Annular Protofibrils
ADDLs	Amyloid derived-diffusible ligands
AUC	Analytical Ultracentrifugation
AFM	Atomic Force Microscopy
Bis-Tris	2-[bis-(2-hydroxyethyl)amino]-2-(hydroxymethyl)propane-1,3-diol
CMC	Critical Micelle Concentration
CD	Circular Dichroism
Dan	Dansyl (5-dimethylaminonaphthalene-1-sulphonyl)
FOs	Fibrillar Oligomers
FITC	Fluoresecin isothiocyanate
Gn-HCL	Guanidine-HCl
LMW	Low Molecular Weight
LFAO	Large Fatty Acid-derived Oligomers
MES	2-(N-morpholino)ethanesulfonic acid
NPN	N-phenyl-1- naphthylamine
NEFA	Non-esterified Fatty Acids
PF	Protofibrils
PMCA	Protein Misfolding Cyclic Amplification

PFOs	Prefibrillar Oligomers
PBS	Phosphate-buffered saline
PAGE	Polyacrylamide gel electrophoresis
R-LFAO	Replicated-LFAO
SFAO	Small Fatty Acid-derived Oligomers
SEC	Size Exclusion Chromatography
SDS	Sodium dodecyl sulfate
ThT	Thioflavin-T
Tris	Tris-(hydroxymethyl)-aminomethane base

CHAPTER I

INTRODUCTION AND LITERATURE REVIEW

Alzheimer's disease (AD) is a progressive and fatal neurodegenerative disorder, which is mostly prevalent in the people above the age of 60.[4] AD is the most common among all neurodegenerative disorders and other forms of dementia. According to recent epidemiological data, it is estimated that around 4.5-5 million Americans are affected by AD, and this figure is predicted to increase to 11-16 million by 2050.[5]

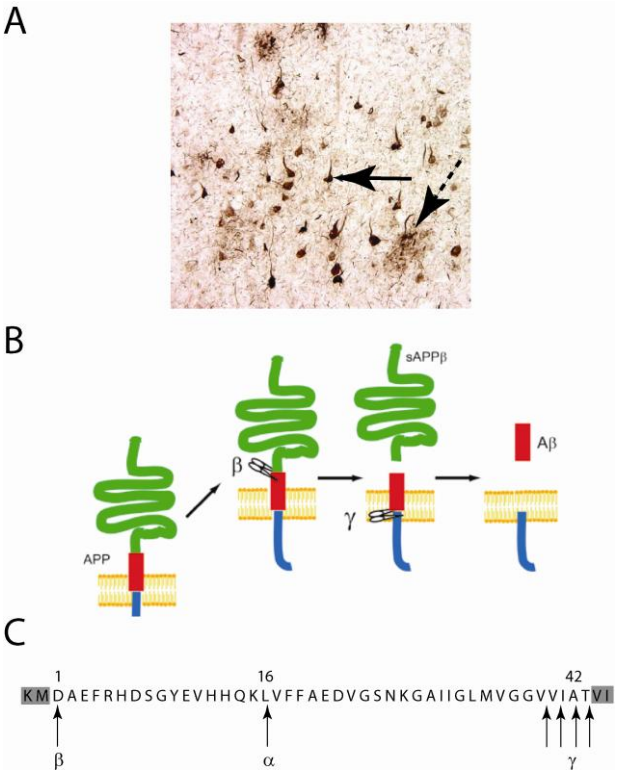

Figure 1. APP Cleavage and Aβ Generation. A) Bright-field immunohistochemistry showing deposits of plaques (dotted arrow) and neurofibrillary tangles (solid arrow) in the AD brain section.[1] B) Schematic representation of extracellular release of Aβ after APP cleavage.[3] C) APP (amyloid precursor protein) amino acid sequence with α-, β- and γ- secretases cleavage sites. The γ secretase can cleave at multiple sites to generate Aβ ranging from 39-43 amino acids.

The deposition of Aβ peptide aggregates primarily in the cortical and hippocampal regions of the brain is mainly responsible for the cognitive decline and memory loss that occur in AD. The two classical hallmarks of the AD brain are neuritic plaques and neurofibillary tangles (Figure 1A). Neuritic plaques are large, proteinacious, extracellular deposits, mainly composed of 40- and 42-amino acid long peptides (Aβ40 and Aβ42, respectively) collectively called amyloid-β (Aβ) peptides. Neurofibillary tangles are intracellular inclusions consisting of the aggregated form of hyper-phosphorylated Tau protein.[4, 6-8] Although both Aβ and Tau are known to be involved in the pathogenesis of AD, Aβ aggregation is largely believed to be the primary neurotoxic event in AD pathogenesis.

Aβ peptides are generated by the sequential cleavage of a ubiquitously expressed, transmembrane protein called the amyloid precursor protein (APP; 770 amino acids) by aspartyl proteases β- and γ- secretase (Figure 1B). The initial cleavage of APP on the N-terminal side by β- secretase generates a large ectodomain and retains a 99-residue COOH-terminal fragment (CTF) within its transmembrane domain, which is then cleaved by γ- secretase, which releases the intracellular domain of APP into the cytoplasm and Aβ in the lumen (Figure 1B).[6, 8,9] The γ- secretase is a multi-subunit protease complex that consists of presenilin-1 or presenilin-2, nicastrin, APH-1 (anterior pharynx-defective 1), and PEN-2 (presenilin enhancer 2).[10] The γ-secretase complex has a wide specificity and can cleave anywhere between the 711th and 714th residues in APP, corresponding to Aβ39 to 43 versions, among which Aβ40 and Aβ42 are the predominant forms (Figure 1C). Alternatively, instead of β-secretase cleavage, another protease called α-secretase

that belongs to the A Disintegrin And Metalloproteinase (ADAM) family of proteases can cleave APP within the Aβ sequence (Figure 1C). This releases a soluble N-terminal domain of APP called P3 containing 83 amino acids which possesses neurotrophic and neuroprotective properties.[6]

AD is largely an idiopathic disorder, but a small percentage is familial, with mutations in specific genes that can lead to excessive deposition of Aβ in brain areas linked to memory and cognitive function.[2] Genetic mutations in APP that lie outside the Aβ sequence (see Figure 2) give rise to early–onset familial AD (FAD).[2] These mutations can lead to an increased production of the longer and more amyloidogenic form, Aβ42.

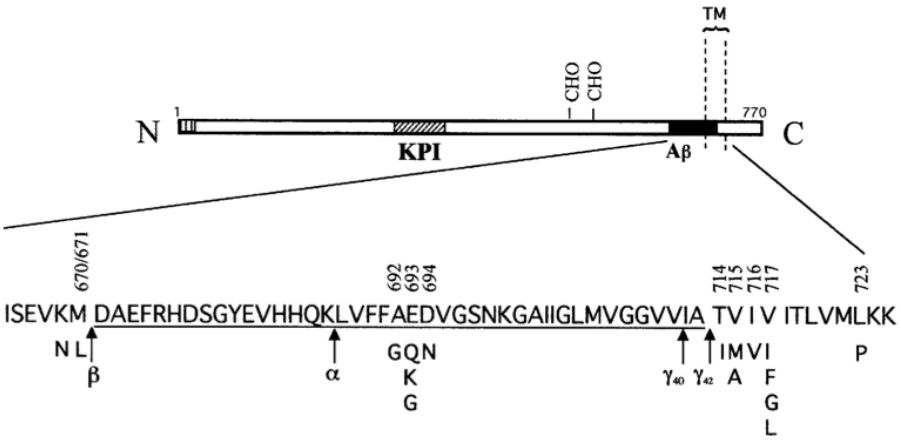

Figure 2. APP Mutations Genetically Linked to Familial Alzheimer's Disease (FAD) or Related Disorders. The sequence within APP that contains the Aß and transmembrane (TM) regions is expanded. The underlined residues represent the Aß1–42 peptide. The vertical dashed lines indicate the location of the TM domain. The letters below the wild-type sequence indicate the currently known missense mutations identified in certain patients with familial AD and/or hereditary cerebral hemorrhage with amyloidosis. Three-digit numbers refer to the codon number according to the ßAPP770 isoform.[2]

Aβ Aggregation

Once generated, Aβ peptides can undergo aggregation, which is a nucleation-dependent process analogous to crystal growth. This process is characterized by the presence of a 'lag-phase', during which prerequisite conformational changes take place, followed by growth-phase towards fibril formation in a sigmoidal pattern (Figure 3).[11, 12, 13] During aggregation, the natively unstructured (random coil) monomeric Aβ undergoes conformational changes that result in a cross-β-sheet structure observed in Aβ fibrils. The lag-phase can be eliminated by adding small amounts of pre-formed aggregates to monomers in a process called 'seeding'.[14]

Oligomers in Aβ Aggregation

Previously, it was believed that Aβ fibrils are mainly responsible for memory impairment and cognitive decline in AD, which led to the formulation of the 'classical amyloid hypothesis'.[15, 16] However this has been widely contested over the years after it became evident that cognitive decline occurred well before emergence of amyloid plaques in transgenic AD mouse brains.[17-22] Several of such observations have resulted in a relatively new amyloid hypothesis that low molecular weight 'soluble oligomers' between ~2-60mers are the primary toxic agents in AD. Consequently, several soluble, low-molecular weight oligomers were identified both *in vivo* as well as *in vitro*, which led to the isolation of many intermediates, including protofibrils (Figure 3).[12, 23-27] Low levels of endogenous, soluble Aβ aggregates present considerable challenges in their identification and characterization; however, several species have been detected in the extracts of human AD brains that run as discrete bands on SDS-PAGE immunoblots.[19, 20, 28, 29] The molecular masses of these bands represent multimers of ~4 kDa Aβ monomers

and range from 2-10mers, and they are collectively called low-molecualr weight, soluble oligomers. It has also been shown that these oligomers are not the broken fragments of larger aggregates that may be formed by SDS during SDS-PAGE analysis.[20, 28] More recently, Shankar and coworkers fractionated the soluble extracts from human postmortem AD brains by superdex-75 size exclusion chromatography (SEC) and showed that dimeric Aβ caused memory impairment and synaptic dysfunction.[29]

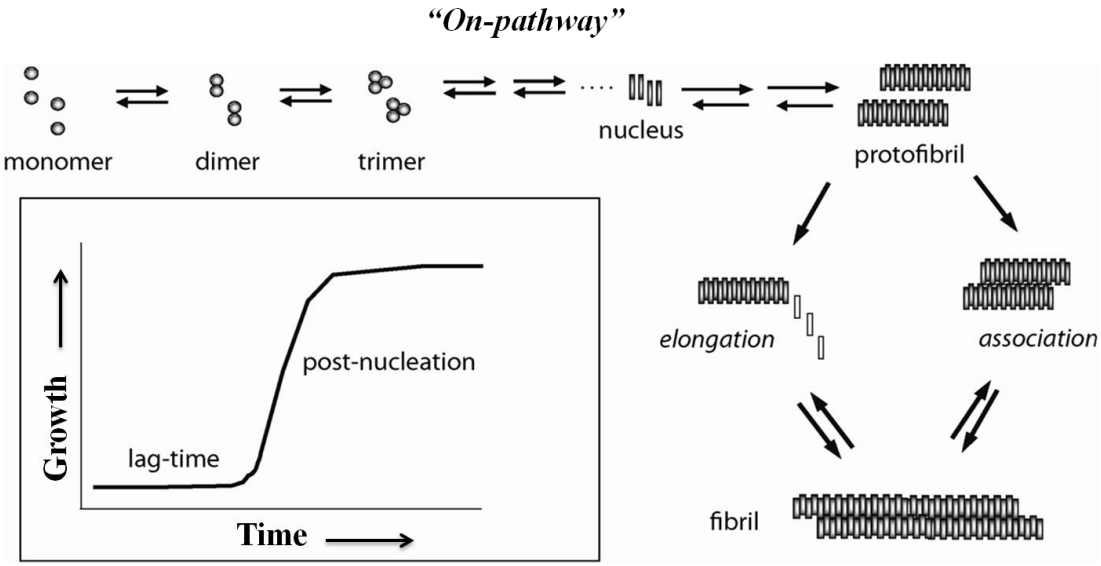

Figure 3. Schematic Representation of Aβ Aggregation 'On-pathway'. (Inset): The sigmoidal growth curve of the Aβ aggregation showing lag-phase and post- nucleation phase.

This hypothesis was further confirmed by the identification of naturally secreted soluble oligomers that inhibit hippocampal long- term potentiation (LTP) in an AD transgenic mouse model and caused impaired cognitive decline.[30,31] LTP is a measure of synaptic plasticity and its inhibition leads to synaptic dysfunction and cognitive decline. Lesńe and coworkers reported that 3-9 month old Tg2576 mice generated a series of oligomeric species with molecular weights corresponding to 6, 9, 12, and 15mers. They

fractionated different species using a Superdex-75 SEC column and determined that a 56kDa (12mer) species, termed as Aβ*56, showed good correlation with the spatial memory deficits in Tg2576 mice.[28] This was the first successful attempt to fractionate endogenous oligomers. They claimed that the 12mers were exclusively responsible for the early synaptic dysfunction and cognitive decline observed prior to the emergence of plaques in AD mice.[28] The soluble oligomers are thought to induce memory loss via synaptic dysfunction prior to cell death.[32]

In another independent work, Townsend and colleagues showed Aβ trimers to be more potent in disrupting LTP than dimmers.[20] They have identified a conditioned medium of the APP V717F-expressing Chinese hamster ovary (CHO) cell lines that form low-number oligomers intracellularly. These naturally secreted soluble oligomers at picomolar concentrations could disrupt hippocampal LTP in the mammalian hippocampus.[20] Podlisnky and coworkers claimed the detection of small amounts of SDS-stable Aβ oligomers in the culture media of CHO cells expressing endogenous amyloid beta-protein precursor genes.[33] These oligomers were primarily identified as dimers and trimers by immunoprecipitation with a panel of Aβ antibodies which included rabbit antisera such as R1280 R1282 and R1963, as well as by electrophoretic co-migration with synthetic Aβ oligomers and amino acid sequencing. Selkoe and co-workers developed protocols for separating secreted oligomers from cell culture by SEC under non-denaturing conditions.[20, 34, 35] They fractionated Aβ monomers and oligomers generated and secreted by conditioned CHO cell medium by SEC and tested them separately on mouse hippocampal slices. They found that trimers are more potent in inhibiting LTP as compared to dimers, suggesting the existence of a level of molecular

specificity in the interaction of Aβ oligomers with neuronal targets. Most recently, Glabe and coworkers shown that fibrillar and prefibrillar oligomers may play a key role in preceding dementia in AD.[36]

Due to their increasing significance in AD pathology, it is becoming imperative to explore and understand the properties of low molecular weight, soluble Aβ oligomers. Endogenous Aβ oligomers are difficult to isolate and are present in extremely low amounts in physiological samples, making biophysical analyses a considerable challenge. Hence, many groups have focused on generating *in vitro* oligomers that can mimic endogenous ones.[28, 29, 33, 36-39] Increasing interest in role of smaller oligomers in AD led to the generation of small diffusible Aβ42 oligomers, referred as Aβ-derived diffusible ligands (ADDLs), which are mostly comprised of Aβ42 4-5mers.[38] The 4-5mers were initially generated by co-incubating Aβ42 with a protein called clusterin and later by simply incubating Aβ42 in DMEM/F-12 hippocampal cell culture medium.[37, 38] ADDLs were toxic to neuronal cells and inhibited LTP in rats.[38] Later, Chromy and coworkers were successfully able to isolate and characterize these ADDLs using SEC and atomic force microscopy (AFM). Results from these experiments indicated that they are fairly homogenous with an average height of ~ 5 nm in AFM.[40] Additionally, fairly homogenous and soluble globular oligomers named 'globulomers' were generated by Barghorn and coworkers, which completely blocked LTP in rat hippocampal slices. In order to generate these, they incubated the Aβ42 peptide in 7 mM SDS initially, diluted the solution to 1.8 mM SDS and dialyzed to remove SDS molecules, yielding globulomers in MW range of 38-50 kDa.[37] Later, they showed that these globulomers are formed via a pathway that was different from the fibril formation pathway, termed as 'off

pathway.[41] Despite reasonable progress on *in vitro* oligomer generation, detailed mechanistic and biophysical information is still lacking, partly due to the difficulties involved in their generation itself.

Amyloid Polymorphism and Structural Classification of Oligomers

Recent studies have shown that amyloid fibrils are polymorphic, that a single polypeptide can fold into multiple amyloid conformations, and factors which can affect the rate limiting nucleation step can dictate the pathway of Aβ aggregation.[42] This feature was first noted with mammalian and yeast prion proteins where it was observed that a single polypeptide can misfold into multiple amyloid conformations.[43] Recently, two types of amyloid fibrils were formed by Aβ40 following aggregation under mildly agitated or quiescent conditions; chemical shift and line-width data from solid-state NMR for 33 of the 40 residues indicated different underlying structures.[44, 45] They also showed that different fibril morphologies may have different underlying molecular structures, which was confirmed by AFM and electron microscopy (EM), that the predominant structure can be controlled by subtle variations in fibril growth conditions, and that both morphology and molecular structure are self-propagating when fibrils grow from preformed seeds.[44, 45]

Furthermore, Glabe and coworkers classified the soluble oligomers into three structurally distinct classes based on their conformation as well as their ability to be recognized by certain conformation-specific antibodies. These classes of oligomers are prefibrillar oligomers (PFO), fibrillar oligomers (FO) and annular protofibrils (APFs), which are recognized by A11, OC and αPF specific antibodies respectively.[36] FOs are small fibrillar fragments which can act as seeds for fibril formation and

elongate/aggregate mainly by monomer addition. In contrast, PFOs are early intermediates of aggregation, specifically recognized by the oligomer-specific A11 antibody. PFOs can align themselves to form protofibrils, which undergo a conformation change to finally form fibrils. Moreover, the N-terminal 6E10 epitope of PFOs has displayed polymorphism in acidic pH, which is completely unobserved at neutral pH.[46] On the other hand, APFs are a completely new and distinct class of oligomers, mainly characterized by pore-like structure and αPF specific antibody. It has been shown that PFOs act as a precursor for APF formation, which are formed by circular arrangement of PFO subunits.[47] These pore-like structure lead to membrane permeabilization and disruption of iron homeostasis causing cell death, a mechanism similar to bacterial pore-forming toxins.[47]

It is abundantly clear that structural variability in Aβ can arise from the conditions in which Aβ is aggregated. Based on Glabe's oligomer classification, several researchers attempted to determine whether the known *in vitro* and *in vivo* oligomers belong to the fibrillar or prefibrillar class of oligomers. It has been observed that the *in vitro* generated oligomers ADDLs and globulomers are not detected by either PFO- or FO- specific antibodies. Interestingly, anti-ADDL and anti-globulomer specific antibodies have shown very high reactivity with Aβ plaque deposits, suggesting that they may have an epitope similar to FOs, fibril type oligomers.[32, 48, 49] In contrast, *in vivo* generated Aβ*56 isolated by Lesné and coworkers belongs to the prefibrillar oligomer class because they have shown high reactivity towards the A11 antibody on immunoblots.[28]

Interfacial Aggregation and Off-pathway Oligomers

Aβ aggregation is a nucleation dependent process as mentioned earlier, and this aggregation process can be affected by environmental factors such as pH, ionic strength, temperature, concentration etc. In addition, the amphipathic nature of Aβ peptide induces preferential aggregation at hydrophilic/hydrophobic interfaces, indicating that interfaces may play a significant role in the Aβ aggregation.[50, 51] Both physiological and non-physiological interfaces are well-known to affect to Aβ aggregation. Nichols and coworkers have unambiguously demonstrated this interfacial phenomenon by showing that Aβ40 aggregation was accelerated by both polar-non polar interfaces as well as by microdroplets of hexafluoro-2-propanol (HFIP). [52, 53]

Physiological interfaces such as those formed by biological membranes and anionic lipids are known to play important role in aggregation and oligomerization.[54, 55] Lipid rafts enriched with gangliosides such as GM1, GD1a, GD1b, and GT1b, along with cholesterol and sphingomyelins, are abundant in the brain and are known to affect Aβ fibrillogenesis.[56-58] These rafts are found largely but not exclusively in cell membrane domains known as caveolae.[55] Importantly, the β, and γ- secretases that generate Aβ peptide from APP, as well as the Aβ peptides themselves, are concentrated in lipid rafts, suggesting that lipids may play pivotal role in Aβ amyloidogenesis.[56-58] Moreover, lipids and lipid metabolites present in amyloid deposits have the potential to affect several areas of amyloid metabolism, including the formation, stability, morphology, and toxicity of fibrils.[59-61] Many studies have focused on lipid bilayers and membrane surfaces where the effect of lipids on Aβ fibril formation is variable and depends on the protein/lipid

ratio and the degree of membrane penetration.[62] But generally it is accepted that Aβ fibril formation is enhanced by the presence of a negatively charged lipid surface.[59, 61, 62] Peroxidized lipids and their derivatives such as 4-hydroxynonenal are involved in promoting Aβ deposition, linking oxidative stress to amyloid deposition.[63] It has also been shown that biological lipids present in the brain can revert inert Aβ plaques or fibrils into highly toxic oligomers, which causes memory deficits in mice.[64] The interaction of sialic acid with Aβ can also promote toxic oligomer formation by inducing peptide conformational change.[65] Furthermore, it has also been observed that neuronal receptors that bind to Aβ oligomers are mainly embedded in lipid rafts, promoting toxicity.[66]

In vitro interactions of Aβ with glycosphingolipids, such as GM1ganglioside, in which micelles and reconstituted liposomes act as rafts to promote Aβ binding and β-sheet structure have been reported.[67-69] Biological membranes can also promote the aggregation of Aβ because of the presence of abundant amounts of phospholipids with polar head groups that can provide an anionic micellar interface. But the interaction of Aβ with these anionic phospholipids/sphingolipid vesicles is limited to polar head groups without penetration of Aβ into bilayer.[70, 71] The rate of Aβ aggregation at an anionic micellar interface can be compared to the rate of aggregation at polar-nonpolar interface using a detergent, sodium dodecyl sulfate (SDS), Although SDS-PAGE analysis is most commonly used as a technique to identify endogenous, soluble Aβ oligomers and SDS is considered as a denaturant that can destroy native protein structure, in low concentrations it can provide an anionic, micellar interface that has been shown to increase Aβ

aggregation.[72] In contrast, SDS concentrations well above the critical micelle concentration (CMC) restrict the peptide in a α-helical structural conformation that does not aggregate.[73, 74] Moreover, Rangachari and coworkers have concluded that Aβ42 rapidly forms oligomers as opposed to protofibrils in concentrations below the CMC of SDS by distinct pathway that they called the "off pathway". These observations indicated that the aggregation pathway depends upon the SDS: Aβ ratio.[73-76]

These published reports indicate that interfaces generated by lipids can alter the Aβ aggregation pathway and, more importantly, can generate toxic oligomers as off-pathway products and play a pivotal role in promoting the exclusive formation of neurotoxic oligomers.

Prion-type Propagation Mechanism –
Conserved Among Neurodegenerative Diseases?

The process of self-propagation is well known among prion diseases, which are also called 'spongiform encephalopathies'. The most common ones are Creutzfeldt-Jakob disease (CJD) and Kuru disease in humans as well as Bovine spongiform encephalopathy (BSE) and scrapie in animals. In prion disease, the normal prion protein in its non-toxic, cellular form, PrP^{C}, converts to a misfolded and infectious scrapie form, PrP^{Sc}. PrP^{Sc} is responsible for the propagation of the disease. Prion propagation is a continuous process, in which newly formed PrP^{Sc} act as template for further initiating the misfolding to continue prion propagation.[77, 78] This 'protein only' hypothesis of prion infectivity was first introduced by Griffith in 1967.[79] It is now believed that a similar protein corruptive mechanism may be also involved in the pathophysiology of other neurodegenerative disorders like Parkinson's disease (PD), frontotemporal lobar dementia (FTLD) and amyotrophic lateral sclerosis (ALS). Desplats and coworkers have shown that α-synuclein involved in PD can migrate and infect neighboring neurons and form lewy bodies, suggesting a prion like propagation mechanism.[80] More recently, Christian and coworkers have shown that extracellular α-synuclein can enter cells by endocytosis and act as 'seed' to promote the aggregation of intracellular α-synuclein in mouse models, further indicating the involvement of prion like corruptive propagation.[81] Similar types of behavior have been also reported for the mutant of superoxide dismutase (SOD1) and TDP43 protein involved in ALS and FTLD, respectively.[82, 83, 84] In the AD field, self-propagation of oligomers is a fairly new and underexplored concept, which requires a great deal more understanding and verification. So far, only a few reports have

been published showing that *in vitro* generated oligomers can undergo replication to generate a similar type of oligomers from monomers on seeding. FOs and PFOs have been shown to undergo self-replication, generating similar type of oligomers from monomer.[85, 86]

Several *in vivo* studies demonstrate that the self-propagation behavior of Aβ amyloids is similar to prions. Jucker and coworkers have shown that brain extract containing Aβ from AD patients or β-amyloid precursor protein (APP) transgenic mice produce cerebral β-amyloidosis and other related pathologies in the transgenic APP mouse model in a time and concentration dependent manner following exogenous induction.[87] Later on, they have also shown that these exogenous seed have similar properties to the PrP^{Sc} form of prion protein.[88] More recently, Stoehr and coworker have shown that Aβ aggregates, whether purified from brain extract or formed from synthetic Aβ, act as prions by inducing widespread cerebral β-amyloidosis.[89] These findings clearly indicate and further support the current hypothesis that 'template-assisted corruptive' protein propagation could be the common mechanism of disease progression and toxicity in all of these neurological disorders. Unfortunately, research so far has been very segregated, failing to give a clear picture of disease pathology and provide a perspective on clinical significance/implications.

Despite the emerging wealth of information regarding soluble oligomers, several molecular level questions still remain that need to be answered. Some of these are:

1. Are there any similarities/dissimilarities between off- and on-pathway intermediates?

2. Is there an underlying mechanism of self propagation and toxicity that is conserved among all neurodegenerative diseases?
3. What is the structure of pathogenic oligomeric seed?
4. Is propagation specific to off-pathway intermediates?
5. Is propagation the property of a specific conformation of seed? If so, what is the optimum threshold concentration of 'seed' required to initiate propagation?
6. What external parameters can affect prion-type propagation?

My current research efforts will be focused on understanding some of these questions, which will provide insights into the mechanism of AD pathology. My findings may also open doors for the development of new diagnostic strategies and help to counteract disease progression through presymptomatic detection and prevention.

CHAPTER II

MATERIALS AND METHODS

Wild type (WT) and Dansyl (Dan) Aβ42 were synthesized by the Peptide Synthesis Facility at the Mayo Clinic (Rochester, MN) using routine Fmoc chemistry. MALDI-TOF mass spectrometry revealed >90% purity of both peptides. SDS and thioflavin-T (ThT) were procured from Sigma (St. Louis, MO). All saturated fatty acids were purchased as sodium salts from NuCheck Prep Inc (Elysian, MN). Monoclonal Ab9/Ab5 antibody specific for Aβ1-16 was supplied by the Mayo Clinic (Rochester, MN). The 1 X 30-cm superdex-75 HR 10/30 SEC column was purchased from GE Life Sciences. Gel electrophoresis and blotting instruments and buffers were procured from Bio-Rad Laboratories, Inc. All other chemicals were obtained from VWR Inc.

Preparation of Aβ42 Monomers

Lyophilized stocks of synthetic Aβ42 were stored at -20 °C, desiccated. Briefly, 1.5- 2 mg of peptide was dissolved in 0.5 ml of 35 mM NaOH and stored for 15 minutes at room temperature prior to size exclusion chromatography (SEC) on a 1 × 30 cm Superdex-75 HR 10/30 column (GE Life Sciences) attached to an AKTA FPLC system (GE Healthcare, Buckinghamshire) to remove any preformed aggregates as previously reported.[90] The column was pre-equilibrated in 20 mM Tris-HCl buffer (pH 8.0) at 25 °C and was run at a flow rate of 0.5 ml/min. One minute fractions were collected. Concentrations of Aβ were determined by UV-Vis spectrometry on a Cary 50 spectrophotometer (Varian Inc) using a molar extinction coefficient of 1450 $cm^{-1}M^{-1}$ at 276 nm (www.expasy.org), corresponding to the single tyrosine residue in Aβ42. Peptide integrity after SEC was again confirmed by MALDI-TOF mass spectrometry. Which

shows a monoisotopic molecular mass of 4516.31 Da in a good agreement with a calculated mass of 4513.13 Da. Monomeric Aβ42 fractions were stored at 4 ^{o}C and used within 2 to 5 days of SEC purification in all experiments to avoid any preformed aggregates in our reactions.

Aβ Aggregation Reactions

All reactions and measurements were made at room temperature unless otherwise noted. Reactions were initiated in siliconized Eppendorf tubes by incubating appropriate concentrations of freshly purified Aβ42 monomer in buffer without agitation. Aggregation kinetic parameters were obtained by monitoring the reaction with ThT and fitting fluorescence data points to the sigmoidal curve in Eq. 1 using Origin 7.0.[91]

$$F = \frac{a}{1+e^{-[(t-t_{0.5})/b]}} \qquad \text{Eq. 1}$$

In this equation t is time, a and b are fixed parameters, and $t_{0.5}$ is the time to reach half-maximal ThT fluorescence. Data points were unweighted. Lag times were equal to $t_{0.5} - 2b$ for each fitted curve.

Measurement of Critical Micelle Concentration (CMC)

CMCs of fatty acids were determined using N-phenyl-1-naphthylamine (NPN) from Sigma (St. Louis, MO) as a fluorescent probe. Fluorescence measurements of NPN in the presence of fatty acids were acquired at the excitation wavelength of 340 nm while scanning emission wavelengths ranging from 400-500 nm on a Cary Eclipse fluorescence spectrometer (Varian Inc.). Fatty acid mixtures contained 0.5-170 mM fatty acid along with 50 mM NaCl in 10 mM Tris buffer, pH 8.0. NPN was added to a total concentration

of 1.5 μM and the solution was incubated for 30 minutes at 37 ^{o}C. The data points were fitted to obtain a linear curve using Origin 7.0.

Seeding Experiments

Monomeric Aβ42 (25 μM) was incubated alone or with different concentration of fatty acids in buffer containing 50 mM NaCl and 20 mM Tris pH 8.0. After 48 hours, 10% (m/v) seed of the incubated sample were withdrawn and mixed with fresh monomeric Aβ42 (25 μM) and incubated at 37 °C under quiescent conditions along with a control without seed. The rate of Aβ42 aggregation was monitored using the ThT assay.

Gn-HCl Denaturation Experiments

The thermodynamic stability of oligomers formed in the presence of fatty acids was determined by guanidine-HCl (GnHCl) denaturation. Aβ42 (25 μM) samples in the presence of specific concentrations of fatty acids (to generate 12-18mers or 4-5mers) were incubated at 37 °C. Aliquots of the samples were taken after 48 hours of incubation, and tyrosine intrinsic fluorescence was measured using λ_{ex} 276 nm and scanning the emission spectrum (λ_{em}) between 300-400 nm with an excitation/emission slit widths of 10/10 nm on a Cary Eclipse fluorescence spectrometer (Varian Inc). The sample was then subjected to denaturation by titrating with 6 M GnHCl within the fluorescence cuvette, at room temperature. The scans were averaged three times to minimize error. Control spectra were measured by adding buffer without fatty acids to buffered 25 μM Aβ42 using the same volumes of GnHCl, which were subtracted from the sample spectra. The area under the curve of the blank-corrected spectra was plotted against the GnHCl concentration. The data were then normalized against the lowest and

highest fluorescence intensity for the given fatty acid concentration. Three such blank-corrected spectra were averaged and are represented here. The resulting curve is fitted using the following Boltzman equation: [92]

$$F = \frac{A_1 - A_2}{1 + e^{(C - C_M)/dC}} + A_2 \qquad \text{Eq. 2}$$

Where, *A1* and *A2* are constants, *C* is the concentration of the denaturant and C_M is the mid-point of the curve, which is considered to be the concentration of *melting*. The data was processed using Origin 7.0.

Preparation and Isolation of LFAOs

Freshly purified Aβ42 (50 μM) was incubated with 50 mM NaCl and 5 mM C12 fatty acid at 37 °C for 48 hours. After 48 hours, the sample was spun at 19,000 x *g* for 20 minutes, and the supernatant was subjected to SEC; the peaks near the void volume (V_o) fractions were collected. Concentrations of collected fractions were determined by UV absorbance with a molar extinction coefficient of 1450 $cm^{-1}M^{-1}$ at 276 nm. All isolated LFAO fractions were stored at 4 ^oC and used within 2-4 days after SEC isolation in all experiments.

Agitation Experiments with Hexane-buffer and Chloroform-buffer Interfaces

To freshly purified 2 μM LFAO or Aβ42 monomer (control) in 20 mM Tris, pH 8.0, 5% (v/v) hexane (ρ = 0.6548 g/ml) or chloroform (ρ = 1.483 g/ml) were added independently and mixed vigorously using a vortex mixer (VWR Inc) for 1 minute of agitation followed by 5 minutes rest. After eight cycles of agitation (~ 1 hour), the samples were then dialyzed against 20 mM Tris-HCl (pH 8.0) at 25 °C using a 2-kDa-MWCO Slide-A-Lyzer G2 dialysis cassette (Thermo Scientific) for 23 hours. Afterward,

the dialyzed samples were subjected to immunoblotting, dynamic light scattering (DLS) and atomic force microscopy (AFM) analyses.

Suspension Experiment with Chloroform-buffer Interface

The suspension method reported previously was followed in our experiments.[93] Freshly purified 2 μM LFAO or Aβ42 monomer (control) (0.3 mL) was suspended on top of 100% chloroform solution (0.3 mL) in a 1.5 mL siliconized Eppendorf tube without mixing. The samples were kept at 25 °C for 24 hours without any disturbance. After 24 hours, the samples were removed just above the interface, without disturbing the interface. The samples from both reactions were subjected to immunoblotting, DLS, and AFM analyses.

LFAO Propagation Experiment

Monomeric Aβ42 (20 μM) was incubated alone or with 2% (0.4 μM) LFAO seed in 20 mM Tris pH 8.0 at 25 °C for 72 hours. Aliquots of the samples were removed at 0, 24, 48 and 72 hours and then subjected to immunoblotting and AFM after spinning at 19,000 x *g* for 20 minutes. The 0.4 μM LFAO seeds alone were used as a control. Similarly, for SEC isolation of replicated LFAO, 50 μM Aβ42 monomer was incubated with 1 μM LFAO under the same conditions, keeping the Aβ42: LFAO ratio the same. Aliquots of samples were removed at 0, 24, 48 and 72 hours and subjected to SEC on a Superdex-75 HR 10/30 column after spinning at 19000 x *g* for 20 minutes to remove fibrils. Fraction 17 from each SEC fractionation at 0, 24, 48 and 72 hours was subjected to immunoblotting and circular dichroism (CD).

LFAO propagation experiment with Dansyl-Aβ42monomer

The above experiment was repeated with Dansyl-Aβ42 (Dan-Aβ42) monomer, which was purified similarly to wild-type Aβ42, as mentioned above. Freshly purified 50 μM Dan-Aβ42 monomer was incubated with 1 μM LFAO under the same conditions as mentioned above. Aliquots of samples were removed after 72 hours and subjected to SEC on a Superdex-75 HR 10/30 column after spinning at 19,000 x *g* for 20 minutes to remove fibrils. Fractions 17 and 18 from the SEC fractionation were subjected to immunoblotting and emission fluorescence spectroscopy using a Cary Eclipse fluorescence spectrometer (Varian Inc.) in scan mode. Dansyl emission was monitored at 450 nm after exciting at 350 nm using 10-nm slits.

Amplification of LFAOs

For Cycle-1, monomeric Aβ42 (50 μM) was incubated with 2% (1 μM) LFAO seed in 20 mM Tris pH 8.0 at 25 °C for 72 hours. After 72 hours, the sample was centrifuged at 19,000 x *g* for 20 minutes to remove any fibrils, and the supernatant was loaded on a Superdex-75 HR 10/30 SEC column to isolate R-LFAOs. Fractions 16 and 17 after SEC fractionation were collected and subjected to immunoblotting to confirm the presence of R-LFAOs. For Cycle-2, 50% v/v R-LFAOs (Fraction 16) were used as seed and incubated with 50 μM monomeric Aβ42 for 96 hours at room temperature. After 96 hours, the supernatant was subjected to SEC after spinning at 19,000 x *g* for 20 minutes to remove fibrils. Fractions 16 and 17 were collected. For Cycle-3, 50% v/v R-LFAOs from Cycle-2 (Fraction 16) were again used as seed and incubated with 50 μM monomeric Aβ42 for 212 hours at room temperature, followed by SEC after spinning at

19000 x *g* for 20 minutes to remove fibrils. The quantitative fold increase after each cycle was calculated by comparing the SEC profile of seeded sample with seed alone.

Generation and Isolation of Replicated LFAO (R-LFAO)

Monomeric Aβ42 (50 μM) was incubated with 5% (2.5 μM) LFAO seed in 20 mM Tris pH 8.0 at 25 °C for 72 hours. After 72 hours, the sample was subjected to SEC onto a Superdex-75 HR 10/30 column after spinning at 19,000 x *g* for 20 minutes to remove fibrils. Fractions 16 and 17 from the SEC fractionation were collected and subjected to immunoblotting to confirm the presence of R-LFAOs.

Determination of LFAO Threshold Concentration for Self-Propagation

Monomeric Aβ42 (30 μM) was incubated alone or with 0.2, 2 and 20% (molar ratio) LFAO seeds in 20 mM Tris pH 8.0 at 25 °C for 212 hours. The aliquots of samples were removed at 72, 144 and 212 hours and subjected to immunoblotting and SEC on a Superdex-75 HR 10/30 column after spinning at 19,000 x *g* for 20 minutes. The molar equivalents of 0.2, 2 and 20% (molar ratio) LFAO seeds alone were also used as a control. The quantitative fold increase after each time point was calculated by comparing the SEC profile of seeded sample with seed alone.

Effect of Temperature on LFAO

Freshly isolated LFAOs (7 μM) was heated at varying temperatures ranging from 10-120 °C for 5 minutes and allowed to equilibrate to room temperature followed by immunoblotting and dynamic light scattering (DLS) analysis. The LFAO's CD spectra were also collected at 10-100 °C in the far UV region with a Jasco J-815 spectropolarimeter (Jasco Inc, Easton, MD). LFAO samples were placed in a 0.1 cm

path-length quartz cuvette (Hellma) and monitored in continuous scan mode (260-190 nm).

To study the effect of temperature on LFAO self-propagation efficiency, monomeric Aβ42 (30 μM) was incubated alone or with 0.6 μM unheated or 80, 100, or 120 °C heated LFAO seeds in 20 mM Tris pH 8.0 at 25 °C for 72 hours. The supernatant samples were then subjected to immunoblotting and SEC on a Superdex-75 HR 10/30 column after spinning at 19,000 x *g* for 20 minutes. The 0.6 μM LFAO seeds alone were also used as a control. The quantitative fold increase after 72 hours was calculated by comparing the SEC profile of seeded sample with seed alone.

Statistical Analysis

Dixon's Q test was applied to the absorbance measurements of the R-LFAOs to remove outliers with greater than 95% certainty. Quantitative fold increase was calculated by dividing the absorbance of the R-LFAO's SEC peaks by the averaged absorbance of at least three measurements of seed alone. Levene's test (95% certainty) was used to test for homogeneity of variance among fold increase, and a one-way ANOVA followed by Tukey's HSD (Honestly Significant Difference) was used to determine confidence intervals for each time/seed combination.

Fluorescence Spectroscopy

ThT fluorescence (F) was monitored in a microcuvette with a Cary Eclipse fluorescence spectrometer (Varian Inc) after 15-fold dilution of Aβ42 samples into 5 mM Tris-HCl (pH 8.0) containing 10 μM ThT. Continuous measurements of F were taken for 1 minute with the excitation and emission wavelengths fixed at 450 and 482 nm respectively, and the excitation and emission slits set at 10 nm.

Dynamic Light Scattering (DLS)

DLS was performed on a Zetasizer Nano S DLS instrument (Malvern Inc., Worcestershire, UK) in Dr. Gordon Cannon's lab (USM). Each sample measurement consisted of 6 runs of 10 seconds each with a pre-equilibration time of 40 seconds. After the measurement, the number (%) was exported and plotted against size (diameter, nm) using Origin 7.0 software.

Polyacrylamide Gel Electrophoreses (PAGE) and Immunoblotting

Samples were dissolved in loading buffer (1X Laemmli buffer) containing 1% SDS, applied without heating to 4-12% NuPAGE gels (Invitrogen) containing bis-Tris, and resolved in MES running buffer with 0.1% SDS. Dye-linked MW markers (Blue Plus2 Prestained Standards, Invitrogen) were run in parallel for calibration. Gels were electroblotted onto 0.45 μm Immobilon nitrocellulose membranes (BioTrace^{TM} NT, Life Sciences Inc). Blots were boiled in a microwave oven in PBS for 2 minutes and were blocked overnight with 1X PBS containing 5% nonfat dry milk and probed (1-2 hours) with 1:1000-1:2500 dilutions of monoclonal Ab9 antibod, which detects amino acid residues 1-16 of Aβ. Blots were then incubated with anti-mouse horseradish peroxide (HRP) conjugate and developed with ECL reagent (Thermo Scientific).

Atomic Force Microscopy (AFM)

AFM was done in our collaborator Dr. Sarah Morgan's lab in the School of Polymers and High Performance Materials at USM. Mica was cleaved using a razor blade and taped to a magnetic sample holder. The mica stub was then covered with a 3-aminopropyl-triethoxy silane (APTES) solution (500 μL APTES in 50 mL 1mM acetic acid) for 15 minutes. The APTES solution was then decanted, and the mica was rinsed

with 150 μL of deionized water four times. After rinsing, the mica stub was dried with compressed N_2 gas and stored in a desiccator for one hour. Next, 150 μL of 0.1-0.25 μM Aβ sample was added to the mica and allowed to adsorb for 20 minutes. The sample was then decanted and the mica stub was rinsed with 150 μL of deionized water four times. Finally, the mica stub was dried with compressed N_2 gas and stored in a desiccator until imaging. The surface topography of each sample was explored by imaging the peptide after it had been adsorbed onto APTES treated freshly cleaved mica. These images were obtained via an Agilent 5500 AFM (Agilent Technologies) in tapping mode, using RTESP-etched silicon probes (length: 125 μm, nominal force constant: 40 N/m, and resonance frequency: 275 kHz) (Veeco Instruments). While under ambient environmental conditions, the scan rate was held constant at 1 Hz. All standard image-processing techniques were performed on Nanoscope version 5.30r2 image analysis software. Nanoscope and Gwyddion version 2.7 software were used to calculate feature heights by two methods: 1) section analysis to extract height profiles and 2) particle analysis to determine the statistical distribution of pixel heights for individual aggregates. Multiple areas were imaged for each sample and while height, phase and amplitude images were collected simultaneously, only representative amplitude images are presented.

Analytical Ultracentrifugation (AUC)

AUC was done in our collaborator Dr. Jack Correia's lab in Department of Biochemistry at University of Mississippi Medical Center (UMMC).

sample preparation. FITC-labeled Aβ42 (FITC-Aβ42) was purchased in a lyophilized form (Bachem Inc.) and stored at – 20 °C prior to use. A stock containing 5 mM FITC-

Aβ42 in DMSO stock was prepared as described previously.[41] The DMSO stock was then diluted to 100 μM in 20 mM Tris (pH 8.0) and used for generating FITC-labeled LFAO (FITC-LFAO). Briefly, for the generation and isolation of FITC-LFAO, 40 μM wild type Aβ42 (WT- Aβ42) and 10 μM FITC- Aβ42 was mixed in 1:4 ratio and incubated with 5 mM C12:0 fatty acid under the same conditions as described above for LFAO preparation, and LFAOs were isolated using a similar protocol. For propagation experiments, monomeric Aβ42 (20 μM) was incubated with 2% (0.4 μM) FITC-LFAO seed in 20 mM Tris pH 8.0 at 25 °C for 72 hours. After 72 hours, the sample was subjected to sedimentation velocity analysis. The 0.4 μM FITC-LFAO seeds alone were used as a control. Similarly, FITC-fibrils were prepared by mixing 45 uM WT- Aβ42 with 5 μM FITC-Aβ42 and incubated with 150 mM NaCl in 20 mM Tris pH 8.0 at 37 °C for 2-3 days. The ThT fluorescence was monitored daily until it reached a plateau. The sample was then centrifuged at 19,000 x *g* for 20 minutes. The pellet was resuspended in 20 mM Tris (pH 8.0) and used for AUC analysis.

sedimentation velocity. Samples were mixed by brief vortexing and then spun in a tabletop centrifuge for approximately 5 seconds to ensure that no sample was lost on the walls of the tube. Samples were then loaded into 1.2 cm path length sedimentation velocity cells (Sedvel60) and placed in an XL-A Analytical Ultracentrifuge modified to accept a fluorescence detection system (Aviv FDS). The temperature on the centrifuge was equilibrated until it remained constant at 20 ^{o}C for at least 5 minutes. The centrifuge was then accelerated to 5,000 rpm, where the focus depth and gain for the fluorescence detection system were adjusted to maximize the signal collected. The centrifuge was then accelerated to 60,000 rpm, and data collection began immediately after final velocity

was reached. Each scan was averaged over 5 consecutive scans to increase the signal to noise ratio. The run was stopped when the fluorescence intensity vs. radial distance profiles remained constant between scans, indicating that the boundary had pelleted. The samples were then re-run for approximately 30 minutes at 60K using absorbance optics to collect pseudo absorbance data. All data was transferred to a separate computer for analysis; the pseudo-absorbance data was used to calculate the meniscus position for each sample using the meniscus wizard in the software program DCDT2+ (version 2.3.2).[94] The software program Sedfit (Sedfit89) was used to generate c(s) distributions for the FDS data with 0.1 S resolution.[95] The c(s) distribution for each sample was integrated and divided by the area, and all data are presented as normalized c(s) distributions. The software program Sedfit was also used to generate *c(M)* distribution after generating the c(s) distribution by assuming a constant diffusion coefficient for all samples and an f/f_o value of 1.2. The *c(M)* distributions were normalized using the same methods as described for c(s) distributions.

Circular dichroism (CD)

CD spectra were obtained in the far UV region with a Jasco J-815 spectropolarimeter (Jasco Inc, Easton, MD). Samples were placed in a 0.1 cm path-length quartz cuvette (Hellma) and were monitored in continuous scan mode (260-190 nm). The acquisition parameters were 50 nm/min with 8 seconds response time, 1 nm bandwidth and 0.1 nm data pitch, and data set were averaged over two scans. Spectra of appropriate blanks were subtracted from data set as indicated. The corrected, averaged spectra were smoothed using the 'mean-movement' algorithm with a convolution width of 25 using the Jasco spectra analysis program.

CHAPTER III

HYPOTHESIS

It is becoming increasingly evident that smaller oligomeric forms (~ 2-50mers) of Aβ aggregates are the primary toxic species in AD. Typically, the intermediates formed along the pathway towards fibrils have been considered as oligomers (Figure 4). However, it has also become evident over the years that Aβ can adopt multiple pathways of aggregation.[41, 46, 75] More importantly, exclusive oligomers can be generated via such alternate, 'off-pathways', which are distinct from the on-pathway of fibril formation.[38, 41, 46, 75] As described in the previous chapter I, it is also well known that environmental factors affect the dynamics of the on- and off-pathways of aggregation, among which interfaces formed by lipids are significant and can promote the formation of oligomers at

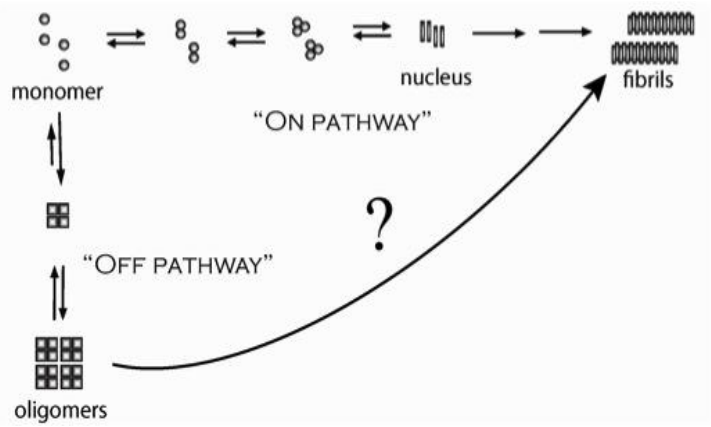

Figure 4. Schematic diagram of Aβ aggregation indicating on- and off-pathways

the cost of fibrils.[96, 97] It is important to understand the pathways of Aβ aggregation because if some oligomers are formed as off-pathway products, their half-life could be significantly higher than the on-pathway ones, which may result in prolonged toxicity to neuronal cells.

We hypothesize that alternate pathways of Aβ aggregation induced by fatty acid interfaces can generate oligomers with unique conformations, resulting in distinct physiochemical and cellular properties.

Specific Research Objectives

Objective 1: To study the effect of various non-esterified fatty acids (NEFAs) on Aβ aggregation and pathways.

We will explore whether anionic interfaces generated by these NEFAs (C9-C12) can form off-pathway oligomers *in vitro* using biophysical techniques.

Objective 2: To isolate and explore the physiochemical properties off-pathway Aβ oligomers generated in the presence of NEFAs.

We will isolate oligomers generated in the presence of NEFAs. Their physiochemical properties will then be explored using biophysical methods and compared with known oligomers like ADDLs, Aβ globulomers, prefibrillar oligomers (PFOs) and fibrillar oligomers (FOs).

CHAPTER IV

RESULTS & DISCUSSION

The Effect of NEFAs on Aβ Aggregation

Based on the existing literature on interfacial aggregation of Aβ as described in the previous sections, we hypothesize that NEFAs will uniquely affect Aβ aggregation in a concentration-dependant manner.

Determination of the Critical Micelle Concentrations (CMC) of Saturated NEFAs

The CMCs of standard NEFAs are well known, but it is not a fix value and can be greatly affected by the presence of slats and other ions in solution. In order to ensure that the buffer and salt conditions (20 mM Tris pH 8.0 and 50 mM NaCl) used for Aβ aggregation do not interfere with their physical properties, e.g. micelle formation, therefore their CMC values were experimentally determined based on a previously published report using N-phenyl-1- naphthylamine (NPN) as a fluorescent probe.[98] NEFAs with varying carbon chain length of C9 (pelargonic acid), C10 (capric acid), C11 (undecylic acid) and C12 (lauric acid) were used in our study (Figure 5A). The normalized fluorescence titration curves for varying concentrations of NEFAs are shown in Figure 5B. The first *inflection point* that occurred upon increasing the fatty acid concentration was considered to be the CMC, as reported. The CMC values determined from Figure 5B were plotted as a function of carbon chain lengths, which showed an expected linear relationship (Figure 5C).

Effect of NEFAs on Aβ42 Aggregation

Previously, it has been shown that varying concentrations of SDS can affect the rate of Aβ aggregation kinetics and can also dictate the aggregation pathway [75]. Based on this and other similar reports, Aβ42 was incubated with three specific concentrations of NEFAs: *a*) below, *b*) near and *c*) above CMC.

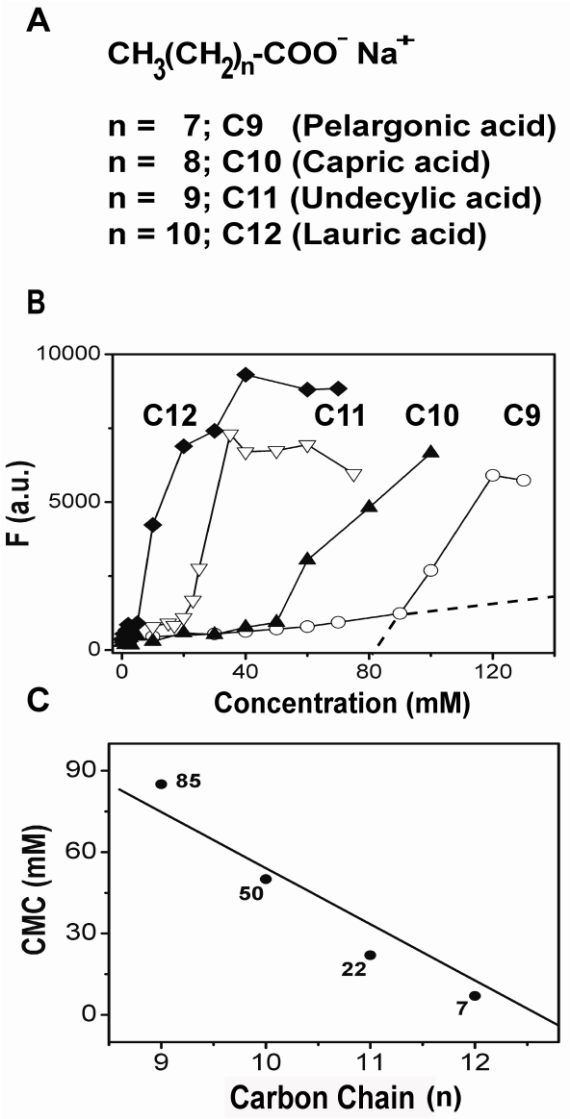

Figure 5. Determination of Critical Micelle Concentrations (CMC). A) NEFAs used in this study: 'n' represents the carbon chain length; B) N-phenyl-1-naphthylamine (NPN) fluorescence response curves for various fatty acids: C9 (○), C10 (▲), C11 (▽) & C12 (◆); C) CMC of various fatty acids plotted as a function of carbon chain length.

Aggregation kinetics of Aβ42 co-incubated with each NEFA was monitored using ThT fluorescence as shown in Figure 6A-D. Aβ42 peptide (25 μM), buffered in 10mM Tris, 50 mM NaCl, pH 8.0 was incubated in the absence of NEFAs at 37 ^{o}C as a control and showed a signature sigmoidal curve of aggregation with a lag time of ~ 58 hours (Figure 6A-D,control).

The concentrations well below CMC for fatty acids (20 mM C9, 10 mM C10, 2 mM C11 and 2 mM C12; ○ in Figure 6A-D) displayed aggregation profiles similar to that of the control. Co-incubation in the presence of NEFAs near their respective CMCs (100 mM C9; 50 mM C10; 20 mM C11 and 5 mM C12; ▲ in Figures 6A-D) showed an augmented rate of aggregation based on ThT fluorescence signals, without significant lag-times as observed in the control sample. On the contrary, Aβ incubations at concentrations above CMC (300 mM C9, 150 mM C10, 75 mM C11 and 20 mM C12; ▽ in Figures 6A-D) seemed to inhibit the rate of aggregation. The data were appropriately blank corrected.

We also removed small aliquots of samples after 130 hours of incubation from the above reactions and subjected them to SDS-PAGE analysis and immunoblotting using the Ab9 monoclonal antibody, which is specific to the Aβ42 N-terminus (Figure 6E). The control Aβ42 incubated alone showed the presence of monomeric and fibrillar (F) bands, which correlates with the observed ThT fluorescence (Figure 6E; lane 2). Likewise, fatty acid concentrations well below CMC showed an identical banding pattern to the control sample (Figure 6E; lanes 3, 6, 9 & 12). For near CMC fatty acid concentrations, a predominant band around 50-80 kDa corresponding to a 12-18mer species (lanes 4, 7, 10 & 13; indicated by triple arrows) was observed, along with

monomeric and fibrillar (F) bands. A faint band around 20 kDa (5mers) was also observed, indicated by double arrows (Figure 6E). On the other hand, incubations above CMC mainly showed the presence of a 16-20 kDa band corresponding to a 4-5mer species (lanes 5, 8, 11 & 14). In addition, a monomeric band was also observed, which could be due to partial dissolution of aggregates by the high SDS concentration during electrophoresis. Similarly, the appearance of the faint 20 kDa band in the case of near CMC incubations could also be due to partial dissociation of 12-18mers.

We have termed these oligomers as 'Large Fatty Acid-derived Oligomers (LFAOs)' for 12-18mers and 'Small Fatty Acid-derived Oligomers (SFAOs)' for 4-5mers, and they will be henceforth called as such. The SDS-PAGE electrophoresis analyses were carried out on 12% bis-Tris acrylamide gels using Laemmli buffer. In sum, it was evident from the data that concentrations near and above CMC, which showed completely different Aβ42 aggregation patterns as compared to the control, predominantly form two distinct oligomeric species: LFAOs and SFAOs, respectively.

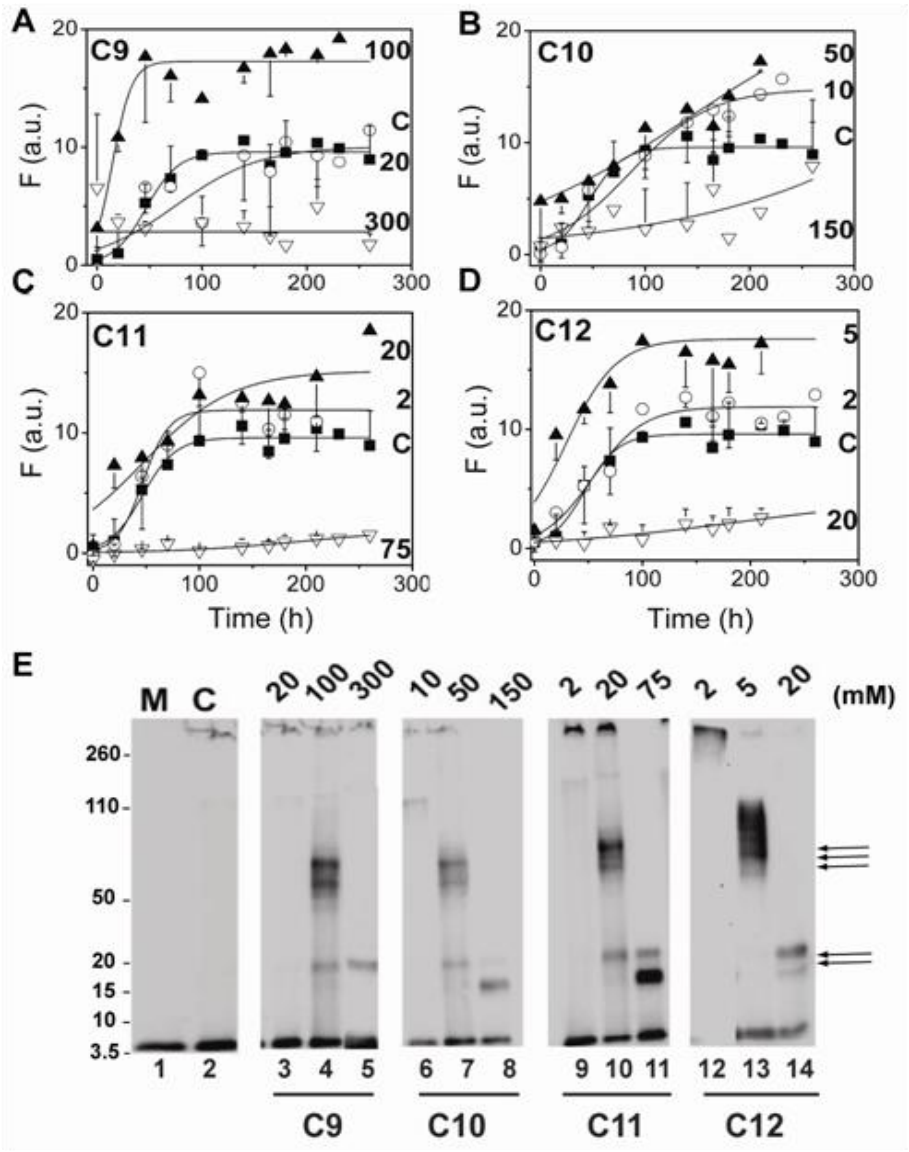

Figure 6. Dependence of Aβ42 Aggregation on Fatty Acid Concentration Monitored by ThT Fluorescence. Monomeric Aβ42 (25 μM) was incubated at 37 °C in buffer alone (■) or with varying concentrations of fatty acids C9 (A), C10 (B), C11 (C) and C12 (D), which are either above (▽), below (○) or around (▲) their respective CMCs. The data was fit with Eq 1; E) Western blots of Aβ42 with varying concentrations of fatty acids after 128 hours of incubation probed using the Ab9 monoclonal antibody. The double arrow indicates SFAOs while the triple arrow indicates LFAOs of Aβ42.

Biophysical Differences Between LFAOs and SFAOs

Next, we studied the morphological and stability differences/similarities between LFAOs and SFAOs using biophysical techniques.

Morphology

Atomic force microscopy (AFM) was used to observe the morphologies of Aβ42 aggregates generated in the presence of NEFAs near and above CMCs. The AFM work was done collaboratively in Dr. Morgan's research group at USM. Small aliquots of sample after 240 hours of the reactions in Figure 6, both near and above CMCs of fatty acids, were removed and deposited on a freshly cleaved mica surface, and AFM images were taken using the tapping mode (Figure 7). As expected, the control sample in the absence of fatty acid showed large fibrillar structures throughout the mica surface (Figure 7A). The measured averaged cross-sectional height was 6.1± 0.8nm for control fibrils, whereas distinct morphological differences were observed between near- and above-CMCs samples. A mixture of fibrillar and smaller rounded/oblong features were observed for near-CMCs samples (Figure 7B, D, F, & H). The measured averaged cross-sectional heights were 5.6±1.3 nm and 7.9±2.9 nm for smaller rounded/oblong and fibrillar features, respectively. In contrast, Aβ samples incubated with NEFAs above CMCs showed only the presence of smaller round/oblong features with a measured averaged cross-sectional height of 6.7±1.0 nm (Figure 7C, E, G & I), and no fibrils were present in the sample. Overall, AFM data suggest that the LFAO and fibril structures formed in near-CMCs samples are morphologically different from SFAOs, predominantly formed in above-CMCs samples.

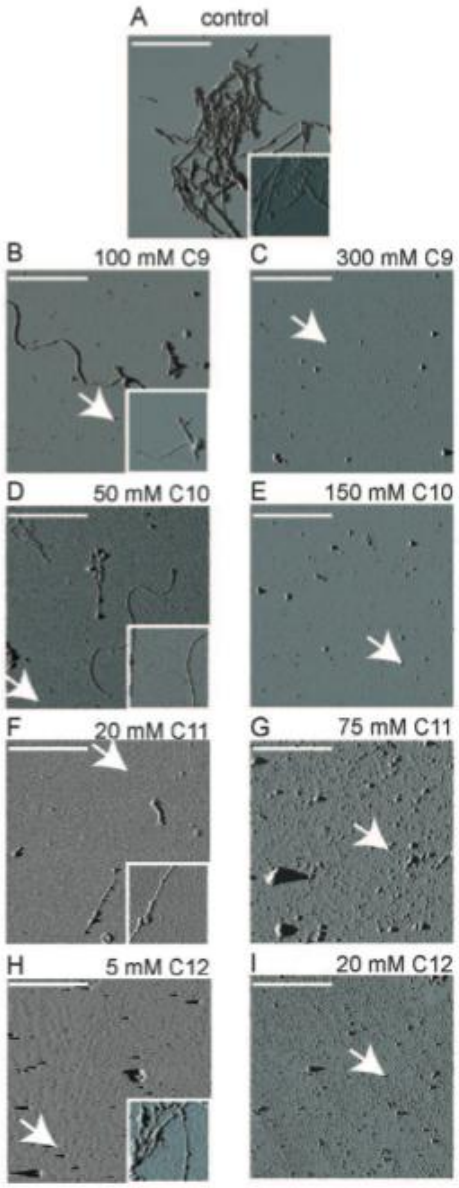

Figure 7. Morphological Differences between SFAOs and LFAOs. Aliquots of the samples from Figure 6 were probed to see the morphologies of Aβ42 aggregates generated in the presence of varying concentrations of fatty acids either near or above CMC by atomic force microscopy (AFM). A) control; B & C) 100 & 300 mM C9; D & E) 50 & 150 mM C10; F & G) 20 & 75 mM C11; H & I) 5 & 20 mM C12. Each square represents 5 x 5 μm. The inset shows a different field with dimensions of 1 x 1 μm.

Seeding Experiments Suggests LFAOs and SFAOs may be Structurally Different

It is evident from ThT fluorescence experiments, immunoblotting, and AFM data that LFAOs and SFAOs may have subtle differences in their structures. As discussed earlier, the lag-time in aggregation can be eliminated by adding preformed 'seeds' to monomeric Aβ.[14] The structure and morphology of the seeded aggregates depend on the nature of seed itself. [99] This means if the added 'seed' has structural similarity with the growing fibrils; the seed will promote and accelerate the formation of the 'on-pathway' fibrils. In previously published reports, seeding experiments were performed to indirectly assess the structural assembly of the seed, and to understand the pathways of

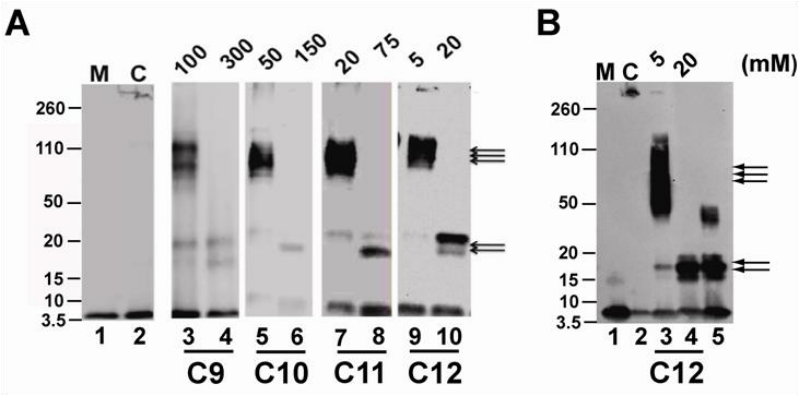

Figure 8: Immunoblot of SFAOs and LFAOs. Western blots of Aβ42 with fatty acids above and near the CMC, after 48 hours of incubation. The double arrow indicates SFAOs, while the triple arrow indicates LFAOs. Monomeric Aβ42 and control (in the absence of fatty acids) are represented by M and C, respectively.

aggregation.[99-102] In our experiments, Aβ42 monomers were incubated with NEFAs to generate LFAOs and SFAOs as described above. After 48 hours 10% (v/v) of the reaction mixture was removed and added to the freshly purified, seed-free monomeric Aβ42 at 37 °C. Small aliquots of the incubated samples were electrophoresed on 12 %

acrylamide gels to ascertain the formation of LFAOs and SFAOs after 48 hours (Figure 8A).

We also compared this to a 4-12% gradient NuPage gel (Invitrogen Inc) to get better separation and resolution of monomeric and dimeric bands as compared to the 12% gel (Figure 8B). No bands were observed between monomer and SFAOs for all the samples, confirming that there were no dimer bands in the incubated samples. A positive control sample containing Aβ42 and 2 mM SDS, which forms 2-4mers, was also included in the gel (Figure 8B, lane 5).[75]

These seeding reactions were also monitored by ThT fluorescence for 100 hours (Figure 9). The 10% (v/v) fatty acid solution was used alone as a control. The 10% (v/v) seeds from the control Aβ42 sample alone showed marginal seeding efficiency as indicated by a slight increase in the rate of aggregation for the seeded sample (Figure 9A). The sample containing LFAOs as seeds rapidly augmented the rate of Aβ42 aggregation as compared to unseeded control samples (Figure 9B, D, F, & H). In contrast, the sample containing SFAOs as seed followed a similar aggregation pattern to unseeded control samples (Figure 9C, E, G, & I).

The results indicate that LFAOs may be structurally compatible with 'on-pathway' fibrils, thereby rapidly promoting their formation by acting as a seed, whereas SFAOs could be structurally dissimilar to LFAOs and fibrils and therefore unable to seed the aggregation of Aβ42. In other words, one could say that the LFAOs and SFAOs may be subtly dissimilar in structure, which causes differences in their seeding behavior.

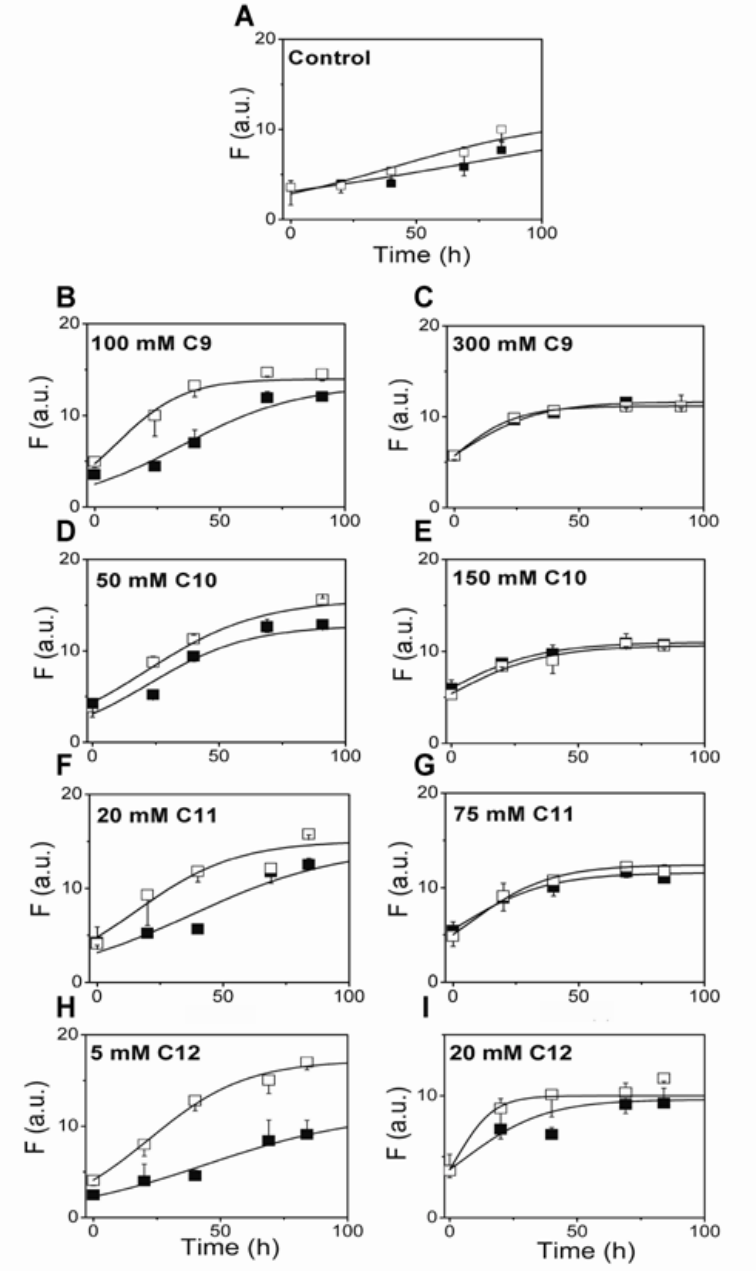

Figure 9. Seeding Experiments with SFAOs and LFAOs. (A-I) Aβ monomer (25 μM) was incubated alone or with 10% (v/v) seed of 48-hour incubated samples of Figure 8A at 37^{o}C and monitored by ThT fluorescence. The figures on the left and right panel represent seeding with LFAOs and SFAOs, respectively. The unseeded control (■) is same reaction as the seeded (□) one, except it lacks seed.

LFAOs and SFAOs have Varying Thermodynamic Stability

Based on the seeding efficiency of LFAOs and SFAOs as observed from the above experiment, it was evident that the oligomers may have different structural assemblies. In order to further confirm this, differences in their equilibrium stabilities was compared by using temporal denaturation melting curves of near- and above-CMC fatty acids incubated with Aβ42, using GnHCl as a denaturant. In this experiment, samples containing LFAOs and SFAOs were titrated with increasing concentration of GnHCl and changes in intrinsic tyrosine fluorescence were monitored at 276 nm (Figure 10). No melting changes were observed upon addition of GnHCl for control monomeric Aβ42, as expected for a natively unstructured protein (■, Figure 10A, B & C). On the other hand, LFAOs and SFAOs formed in near- and above-CMCs, respectively, showed a significant shift in fluorescence intensity with low GnHCl concentrations followed by a gradual decrease in intensity to almost the level of control monomeric Aβ42 with increasing GnHCl concentrations (○ & ▲; Figure 10). Only the melting curves for C10, C11 & C12 were shown in Figure 10 because the first four or five data points collected for C9 at low concentrations of GnHCl were inconsistent, especially due to high concentration of fatty acids. It is possible that initial addition of low concentration of GnHCl can cause precipitation of fatty acids, resulting in erratic data points followed by stabilization of the solution at higher concentrations. Because of this, it was very hard to collect reliable data for C9 near- and above-CMCs samples. It was observed that LFAOs melted earlier than SFAOs in case of all three fatty acids C10, C11 & C12 (Figure 10). The apparent melting denaturant concentration (C_M) values for LFAOs (○; Figure 10) were 1.94 ± 0.05, 0.87 ± 0.1 and 1.86 ± 0.04 M for C10, C11 and C12, respectively. In

contrast, SFAOs required a higher concentration of GnHCl for melting. The C_M values for SFAOs (▲; Figure 10) were 2.55 ± 0.03, 2.38 ± 0.06 and 3.83 ± 0.09 M for C10, C11 and C12, respectively.

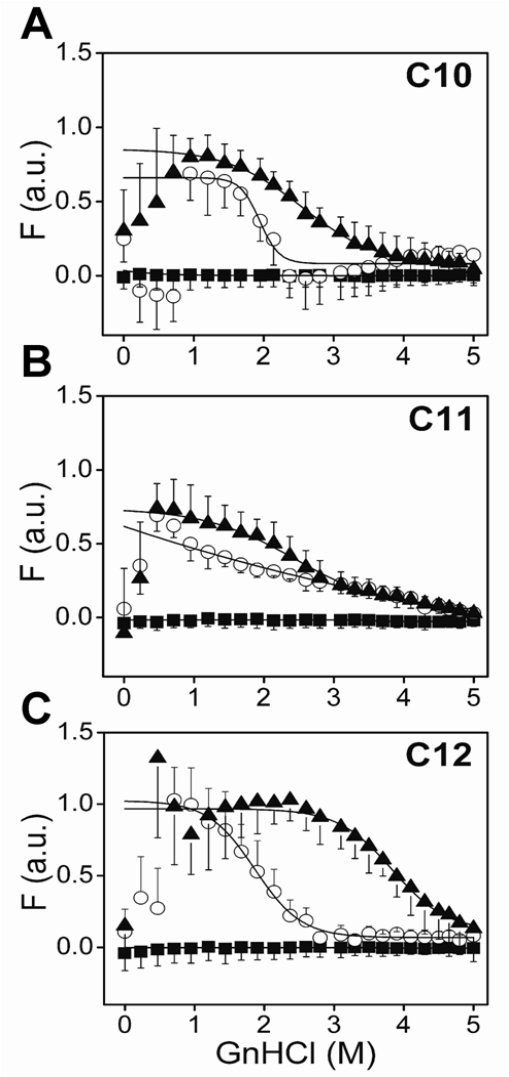

Figure 10. Thermodynamic Stabilities of SFAOs and LFAOs determined by GnHCl Denaturation Experiments. Aβ42 (25 μM) was incubated alone (■) or with NEFAs C10 (A), C11 (B) and C12 (C) in similar conditions as Figure 11 at concentrations near (○) and above (▲) their CMCs. Three scans were averaged and the areas under the peaks were normalized and plotted against GnHCl concentrations. The data was fit using Boltzman's sigmoidal fit (Eq. 2) by Origin 7.0. Three data sets were averaged.

To rule out the possibility of a *shielding effect* by the high concentration of fatty acids required for SFAO generation, a negative control experiment with a 7 kDa non-aggregating protein called human granulin A (Grn-A), comparable in size to Aβ42, was performed in similar manner (data not shown).[103] The data obtained showed that there is a slight shielding effect in higher fatty acid concentrations as compared to lower concentrations, and this difference in melting concentrations was very low compared to the difference between LFAOs and SFAOs. It was also interesting to observe that the SFAOs formed in C12 fatty acid appeared to be more stable than SFAOs of C10 & C11 fatty acids. Overall, the data showed that SFAOs are more stable than LFAOs and complement the previous data, which indicated that these two oligomeric species may be structurally different.

Discussion

It is well known that interfaces, whether physiological or non-physiological, can have profound effect on Aβ aggregation. The interaction of Aβ42 with medium-chain saturated NEFAs has provided useful insights about the phenomenon of interfacial aggregation. The data presented here clearly indicate that different concentrations of fatty acids can dictate multiple pathways of Aβ aggregation. Interestingly, the pathway adopted by Aβ mainly depends on the nature of interface (non-micellar/micellar) generated by specific concentrations of NEFAs, not by the type of fatty acid used. In other words, the same type of LFAOs or SFAOs were generated by near and above CMC fatty acids irrespective of the carbon chain length, indicating that concentration relative to CMC plays a crucial role in dictating pathways. This is evident from the observation that a similar concentration of 20 mM has completely different Aβ aggregation profiles in the

cases of C9, C11 and C12, but the Aβ:NEFA ratio was constant in all cases (Figure 6). 20 mM concentration (well below CMC) in the case of C9 does not affect aggregation, but on the other hand the same 20 mM concentration forms LFAOs (near CMC) and SFAOs (above CMC) in the cases of C11 and C12, respectively (Figure 6E). Moreover, an increase in the formation of fibrils was observed at a fatty acid concentration near the CMC, which forms LFAOs, when Aβ:NEFA ratios were increased (Figure 11). Similarly, when Aβ:NEFA ratios for fatty acid concentrations greater than CMC, which form SFAOs, were increased, the formation of LFAOs was observed (Figure 11), indicating that apart from CMC, ratios of Aβ:NEFA are also crucial in dictating the pathways and nature of oligomers formed.

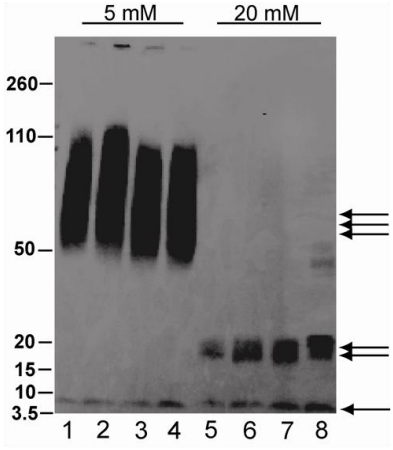

Figure 11. Incubation of 5 & 20 mM C12 with Varying Concentrations of Aβ42 ; lanes (1-4) 5 mM C12 with 12.5 μM , 25 μM , 50 μM , 75 μM Aβ42 respectively ; lanes (5-8) 20 mM C12 with 12.5 μM , 25 μM , 50 μM , 75 μM Aβ42 respectively.

LFAOs and SFAOs Are Kinetically Trapped Off-pathway Intermediates

LFAOs were generated within 24-48 hours of incubation of Aβ42 with near CMC concentration of fatty acids at 37 °C and remained stable for at least 10 days. The increased ThT fluorescence observed with LFAOs causes doubt as to whether it arises

from LFAOs or some fibrils that may be present (Figure 7). To complicate the issue, we know that LFAOs are structurally similar to fibrils, as they were able to seed Aβ42 fibril formation (Figure 9).

However, two separate experiments indicated that they might be *off-pathway* intermediates. First, they remained stable even after ~500 hours of incubation, which is unlikely for on-pathway intermediates (Figure 12A). Secondly, known fibril inhibitors like Congo Red and Rifampicin failed to inhibit the formation of LFAOs (Figure 12C).[41, 46] Conversely, seeding experiments suggested that LFAOs may have structural similarities with on-pathway fibrils because of their seeding efficiency (Figure 9), and also NEFA free, isolated LFAOs slowly converted to fibrils after ~500 hours incubation at 37^{o}C (Figure 12B). Together, the data suggested that LFAOs might be kinetically trapped as *off-pathway* oligomers in the presence of NEFAs, but after isolation (removal of fatty acid, elaborated in the next section) they slowly convert into on-pathway fibrils by associating with themselves (Figure 12). But since the conversion to fibrils of LFAOs free of associated NEFAs occurs at a very slow rate, it is likely that LFAOs are kinetically trapped *off-pathway* oligomers.

On the contrary, SFAOs formed above CMC concentration clearly indicated that they are off-pathway species. They failed to show any increase in ThT fluorescence and also completely failed to convert to fibrils even after ~500 hours of incubation (Figure 12C). Moreover, SFAO samples were fairly homogenous and without any fibrils as observed by AFM images (Figure 6E and 7). And no increase in the rate of aggregation was observed on seeding; indicating that they might be structurally incompatible with on-pathway fibrils, which further complements the finding that they are off-pathway species.

Unfortunately, all attempts to isolate SFAOs using SEC like LFAOs were unsuccessful; therefore the seeding efficiency of isolated SFAOs was not evaluated.

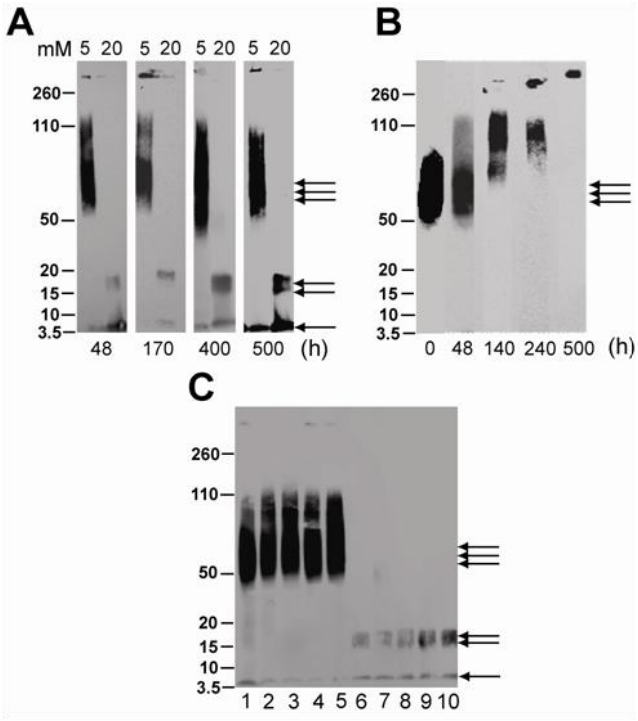

Figure 12. Oligomeric LFAOs as well as SFAOs are Formed Along 'Off-pathway'. All samples were electrophoresed on 4-12 % NuPage gels with MES running buffer. A) Immunoblots of incubations of buffered 25 μM Aβ42 with 5 and 20 mM C12 for ~500 hours at 37 °C similar to Figure 11. Double and triple arrowheads indicate SFAOs and LFAOs respectively; B) Immunoblots of SEC fractionated LFAOs (9 μM) of Aβ42 (Figure 20) in 20 mM Tris-HCl, 50 mM NaCl, pH 8.0 incubated at 37°C for the indicated times; C) Effect of fibril inhibitors like Congo red (CR) & Rifampicin (Rfn) on Aβ42 oligomer formation. Lanes 1-5 show 25 μM Aβ42 incubations with 5 mM C12: lane 1 – with no inhibitors, lane 2 and 3 – with 6- and 8-fold molar excess of CR, lane 4 and 5 – with 6- and 8-fold molar excess of Rfn. Lanes 6-10 show similar 25 μM Aβ42 incubations with 20 mM C12: lane 6 – with no inhibitors, lane 7 and 8 – with 6- and 8-fold molar excess of CR, lane 9 and 10 – with 6- and 8-fold molar excess of Rfn.

Together, the data suggested that both LFAOs and SFAOs are transiently trapped as *off-pathway* oligomers. It is also possible that fatty acid might play an important role in stabilizing the structure of oligomers, and their removal may have a destabilizing effect on oligomers.

The exact nature of the Aβ-NEFA interaction is unclear at this time. However, a rough model portraying the possible mechanisms of Aβ-NEFA interaction based on the above results is shown in Figure 13. If non-micelle ⟷ micelle was assumed to be a determined reaction with the equilibrium constant, K_D, being equal to the CMC value, then it is obvious that above the CMCs, Aβ mainly interacts with the micellar form (Figure 13). Based on our observation of SFAO formation, it seems likely that the anionic interface provided by micelles accommodates 4-5 Aβ monomers. These SFAOs seem to be thermodynamically more stable (stabilized by micelles) than LFAOs (Figure 10). Interestingly, no effect on Aβ aggregation was shown with non-micellar concentrations of NEFA (<<CMC) (Figure 6). Near the CMC concentration, a dynamic equilibrium exists between non-micellar ⟷ micelle transitions, which seems to exert a unique effect on Aβ aggregation. Near CMC, no well-defined interface forms, this may result in different modes of interaction between Aβ and fatty acids (Figure 13). In other words, LFAOs may be kinetically trapped intermediates along the 'off-pathway' as compared to thermodynamically stable SFAOs.

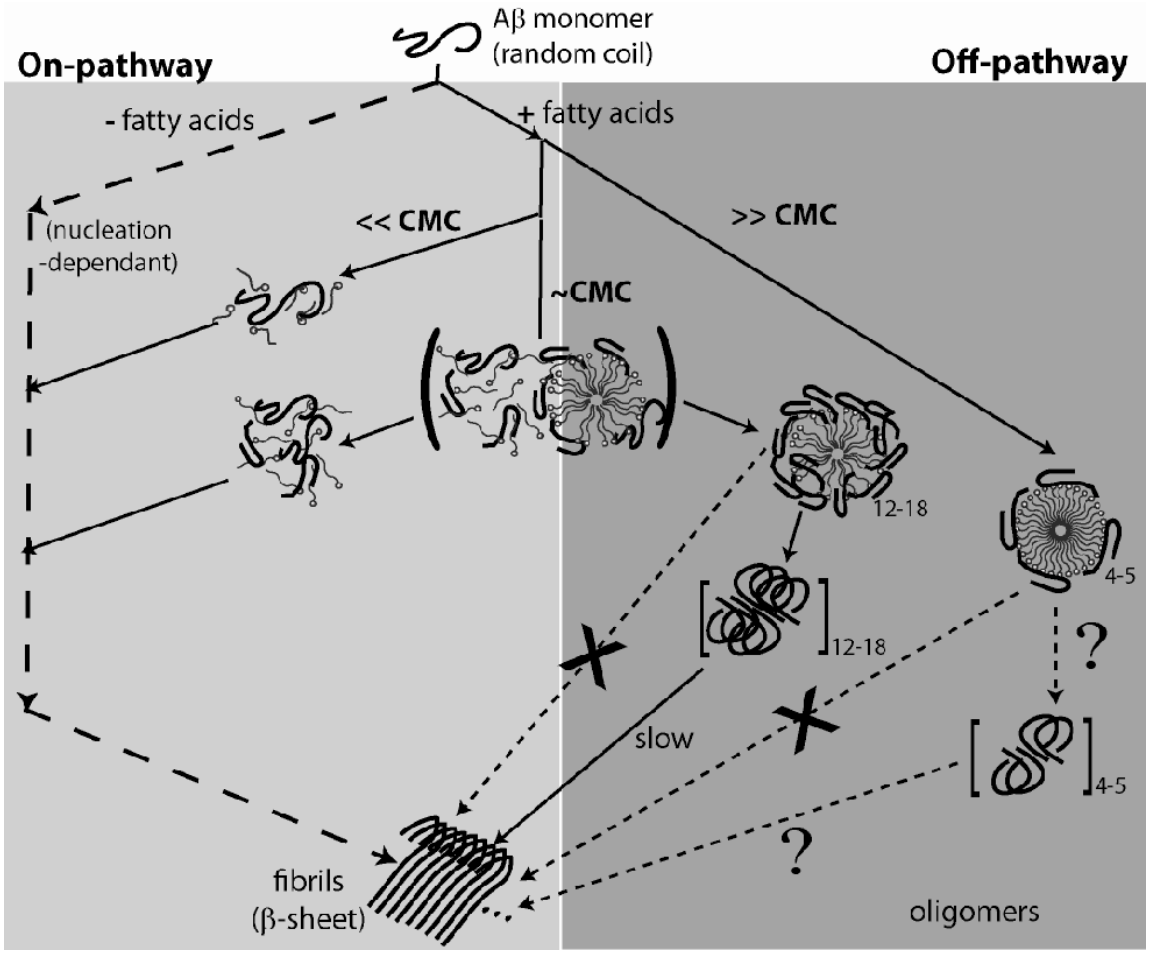

Figure 13. Schematic Model of Aβ42 Aggregation Pathways in the Presence of NEFAs Based on the Data Obtained in the Study. The square brackets indicate isolated oligomers while the question marks indicate that these parts were not explored in this study.

Physiochemical Properties and Self-propagation of LFAOs

LFAOs and SFAOs generated in the presence of 5 and 20 mM C12 fatty acid respectively were isolated using SEC to further explore their stability in the absence of fatty acid, physiochemical properties and prion-type self propagation behavior.

Isolation of Oligomeric LFAOs and SFAOs

In order to further characterize these oligomeric species, it was very important to isolate them, free of monomers, fibrils and fatty acids. This will help in understanding and exploring the molecular features of these specific oligomeric species and provide information about their stability in the absence of fatty acids. To do so, 50 μM Aβ42 was incubated with 5 or 20 mM C12 fatty acid for 48 hours to generate LFAOs and SFAOs respectively, as shown in Figure 6E (Chapter IV.1). After 48 hours, LFAOs (incubation with 5 mM C12) were subjected to SEC using a Superdex-75 column (see next subsection VII). The presence of residual NEFAs present, if any, in the isolated LFAO fractions was quantified using a free fatty acid assay kit (BioVision Inc., Milpitas,CA) method as published previously.[104] This experiment indicated a negligible amount (<0.1%) of NEFA was present in fractions containing isolated LFAOs (Figure 14). The results clearly suggest that LFAOs can maintain their structural integrity even after isolation and removal of fatty acids. Attempts to isolate SFAOs using SEC were unsuccessful (data not shown) and hence, were not further pursued.

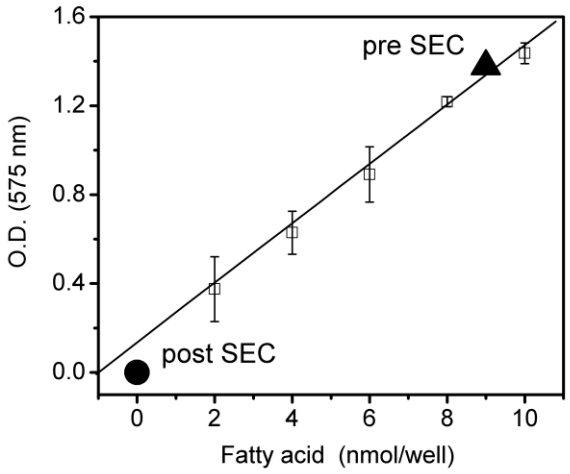

Figure 14. Quantitation of NEFA Content in Isolated LFAOs: The amount of NEFA associated with LFAOs before and after SEC fractionation was estimated using free fatty acid quantification kit. The experiment was performed as per the manufacturer's instructions. Briefly, a standard curve was generated by adding 2 µl aliquots of a known concentration of palmitic acid to each well containing the reaction mixture provided by manufacturer (□). The reactions were monitored colorimetrically at 570 nm. The concentration of NEFA present in 2 µl aliquots of LFAOs before (pre SEC; ▲) and after (post SEC; ●) isolation by SEC were estimated using standard curve. Based on this analysis, NEFA concentration before SEC was estimated to be 4.5 mM, which is comparable to the 5 mM used. On the other hand, for the isolated LFAO, a negligible amount of NEFA was detectable in the sample, suggesting a complete removal of NEFAs from LFAOs upon fractionation.

LFAOs are Disperse Oligomers

The isolation of LFAOs generated in the presence of 5 mM C12 and their molecular size distribution were estimated using SEC and analytical ultracentrifugation (AUC), respectively. The Aβ42 was incubated with 5 mM C12 fatty acid at 37 °C for 48 hours to generate LFAOs as described (Figure 6E; Chapter IV.1) and subjected to fractionation on a Superdex-75 SEC column (Figure 15A, smooth line). The samples eluted in two major peaks, one between fractions 17 and 20 and the other between fractions 22 and 25. A small extra peak was also observed near the void volume (fraction

16) of the column. The LFAOs are eluted in the partially included volume fractions 17 and 18 as compared to monomers, which eluted in fractions 22-25. The SEC profile of LFAOs was compared with those of globular protein standards (gel filtration standards, Bio-Rad) to estimate the molecular mass of LFAOs based on retention volume (data not shown). Based on this analysis, the molecular mass of LFAOs was estimated to be between 60 and 200 kDa. Additionally, Aβ42 protofibrils (PFs), which have a molecular mass >200 kDa were also subjected to fractionation under similar condition as LFAOs.[105, 106] The SEC profile of PF sample mainly showed two elution peaks, one at the void volume at fraction 15 (V_o; Figure 15A, black arrow) for PFs and second for monomers at fractions 22-25 (Figure 15A, dashed line). The SEC fractionation of PFs further supplemented our observation with globular protein standards that molecular mass of LFAOs is between 60 and 200 kDa. The AFM of the isolated LFAOs mainly showed a bimodal distribution of non-fibrillar punctuate dots like structures with an average height ranging from 7-10 and 16-19 nm (Figure 15A, inset).

The sedimentation velocity experiments in an analytical ultracentrifuge were performed to estimate the molecular size distribution of LFAOs. The AUC experiments were done in our collaborators Dr. John Correia lab at UMMC. For these experiments, FITC-Aβ42 was introduced into LFAOs assembly (as described in the Materials and Methods, Chapter II) to facilitate monitoring by fluorescence detection system (FDS).

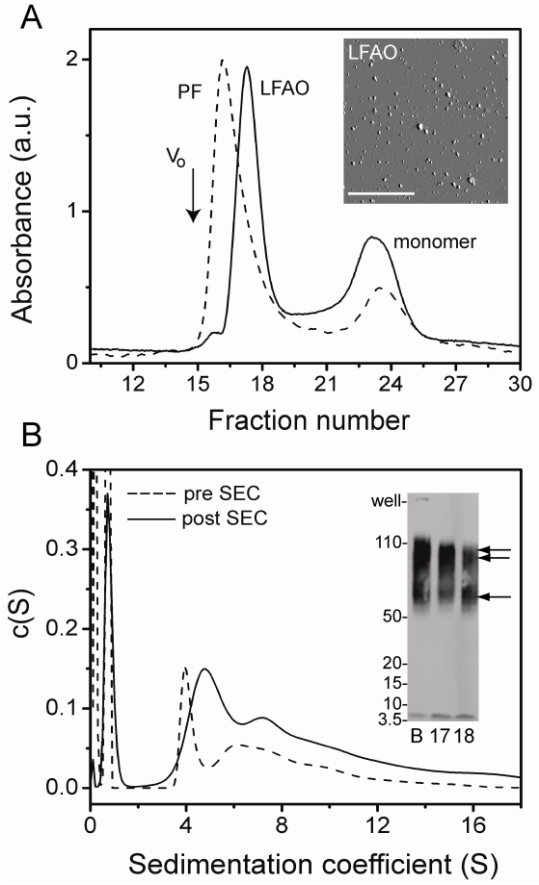

Figure 15. Isolation and Characterization of LFAOs. A) The SEC fractionation of LFAOs using a Superdex-75 column in 20 mM Tris pH 8.0 at room temperature with a flow rate of 0.5 mL/min and a fraction size of 0.5 mL. As a comparison, a sample of protofibrils (PFs) of Aβ42 was as also fractionated. V_o indicates the void volume based on globular protein standards. (Inset): AFM image of fractionated LFAOs. Scale bar represents 2.5 μm. B) Normalized c(S) distribution profile generated from a sedimentation velocity experiment performed at 50,000 x *g*. (Inset): Immunoblot of LFAOs before and after fractionation. Single arrow indicates 50-70 kDa bands while double arrow indicates 80-110 kDa bands.

In AUC, the rate of sedimentation of macromolecules was monitored in the presence of centrifugal force, which allows the determination of their hydrodynamic radius and thermodynamic properties in solutions.[107] AUC is the method of choice to determine the exact molecular mass of proteins and their complexes and also to study

protein self-assembly and heterogeneous interactions like protein-protein, protein-DNA and protein-small agents.[107]

Labeling with FITC reduces the amount of sample needed and facilitates detection at very low concentrations. The *c(S)* sedimentation coefficient distribution profile, which helps to model the hydrodynamic radii of proteins and their complexes in solution, of LFAOs before and after fractionation was analyzed to observe any size differences (Figure 15B). The Aβ42 sample incubated with 5 mM C12 before fractionation when subjected to AUC showed a distribution of multiple peaks with a sharp peak centered on 4 S and a more disperse peak between 6 and 12 S with a additional peak at ~ 1 S (Figure 15B, dotted lines). The 1 S peak corresponds to monomeric Aβ42 as determined by running a control sample (Figure 16A), and SEC fractionated LFAOs (fraction 17) showed an almost identical AUC profile as the unfractionated sample, with a main peak centered at 5 S and a second disperse peak between 7 S and 12 S, along with a monomeric 1 S peak (Figure 15B, smooth lines). The LFAOs showed a similar peak distribution even after 10- & 50-fold dilutions (data not shown). A relative decrease in the amount of monomers was also observed after SEC: 52.3% and 14.3% monomers before and after fractionation, respectively. The Aβ42 fibrils were also analyzed by AUC to compare with LFAOs; they on the contrary showed a heterogeneous mixture of large species between 40 and 200 S (Figure 16B). The immunoblots of the LFAO sample both before and after SEC primarily showed a disperse band between 56 and 110 kDa with two distinct band distributions; one is around 56-70 kDa and other is centered at 80-110 kDa (Figure 15B, inset). The immunoblot band distribution further complements the bimodal distribution observed in AFM and AUC

data. Together, the data suggest that LFAOs are not discrete, but a disperse mixture of oligomeric species.

LFAOs are Self-propagating Oligomers

Prion proteins are well known to undergo corruptive template assisted self replication by converting normal prion proteins (PrP^{C}) to misfolded (PrP^{Sc})form.[77] Recent studies have shown that a prion-type propagation mechanism is also involved in the pathogenesis of other neurodegenerative diseases like PD, FTLD and ALS.[80-84] But prion type self-propagation is a relatively new and unexplored area in the AD field, and so far only two oligomeric species of Aβ, prefibrillar (PFOs) and fibrillar oligomers (FOs), have been shown to possess a self-propagating property upon interaction with monomeric Aβ.[85, 86] Therefore, we want to explore whether LFAOs can self-propagate upon monomer addition.

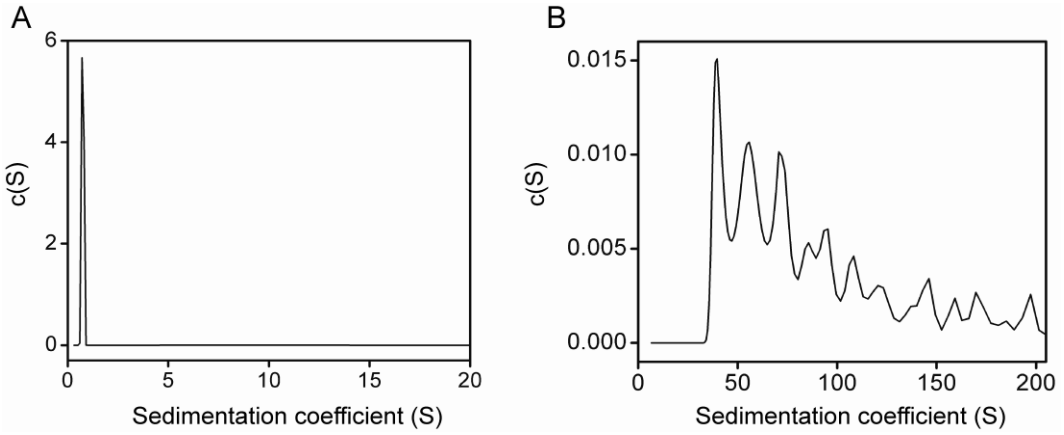

Figure 16. AUC of Monomer and Fibril. A *c(S)* distribution profile generated from sedimentation velocity experiments for Aβ42 monomers (A) and fibrils (B).

For this experiment, 20 μM freshly purified, aggregate-free, monomeric Aβ42 was incubated with 0.4 μM (2% molar ratio) isolated LFAOs as a seed at ambient temperature, and the reaction's progression was monitored with ThT, immunoblotting

and SEC. Small aliquots of samples were removed at 24, 48 & 72 hours and subjected to SDS-PAGE and immunoblotting. The amount of sample loaded in each lane was kept constant at 28 ng based on the initial concentration of LFAOs seed (Figure 17A), for the approximate quantification of the blots. The immunoblot clearly showed a more intense LFAO band centered around 100 kDa within 24 hours compared to the 0 hour sample (lane 3). The 100 kDa band represents the higher molecular weight species of LFAO (80-110 kDa) from the two species observed for isolated LFAOs (lane C), and the lower molecular weight species (~56-70 kDa) was completely absent (Figure 17A; 24 hours). A progressive increase in the 100 kDa band intensity was observed after 48 and 72 hours, along with a continuous decrease in the monomer band intensity, indicating that monomers were being converted into more LFAOs (Figure 17A; 48 and 72 hours). Moreover, a large molecular weight species was also observed at the top of gel after 72 hours (lane T; 72 h), which was absent in the supernatant sample loaded on the gel after centrifuging the sample for 20 minutes at 19,000 x *g*, suggesting the formation of fibrils. Some degree of fibril formation was expected because it is likely that besides monomer-LFAO interactions, monomer-monomer interactions occur in parallel, leading to on-pathway fibrils. The propagation reaction was also monitored by ThT fluorescence (Figure 17C). The Aβ42 seeded with 2% LFAOs (Figure 17C,○) showed a lag phase of ~72 hours as compared to control ~84 hours (Figure 17C, ■), indicating a relatively insignificant amount of seeding. But a significant amount of seeding (reduction in lag phase) was observed with 20% seed in our previous experiment (data not shown). A significant amount of LFAOs was also observed in the seeded sample immunoblots run during the lag phase (24, 48 and 72 hours), which was not seen in the control (Figure

17A). This clearly suggests that the propagation of LFAOs mainly occurred during the lag phase. Notably, immunoblots showed that the propagation reaction occurring upon seeding with LFAOs only leads to the formation of 80-110 kDa oligomeric species at the expense of the 56-70 kDa species observed in LFAO seeds.

In order to confirm that propagation leads to a quantitative increase in LFAOs that would occur in a self-propagating event, SEC was used. Aβ42 (50 μM) was seeded with 2% LFAOs (1 μM) and incubated for 72 hours. Immunoblots after 24, 48 and 72 hours of incubation confirmed propagation process as shown in Figure 17A. The samples were subjected to SEC fractionation after the indicated times. Fractions 16-19 showed the presence of propagated LFAOs on immunoblots (Figure 17B). A ~4-fold increase in the amount of LFAOs was observed in SEC, as shown by absorbance in comparison with non-seeded sample fractions after 72 hours (Figure 17D). The Far-UV CD of SEC fraction 17 at 24, 48 and 72 hours points also showed a progressive increase in β-sheet conformation, further complementing the observation of an increase in LFAO amount upon seeding (Figure 17E). The formation of 80-110 kDa species upon seeding that seemed to occur at the cost of 56-70 kDa species was confirmed by sedimentation velocity analysis before and after 72 hours of propagation cycle at room temperature (Figure 17F). The sample after propagation showed a significant peak shift towards ~80-110 kDa species (Figure 17F, smooth line), which supported the immunoblot data (Figure 17A) and consolidated the observation that the high molecular weight ~80-110 KDa species was predominantly formed upon propagation. A slight decrease in the amount of monomer ~6 % was also observed in the seeded sample AUC data (Figure 17F), further

strengthening the observation that propagation leads to quantitative conversion of monomer to LFAOs.

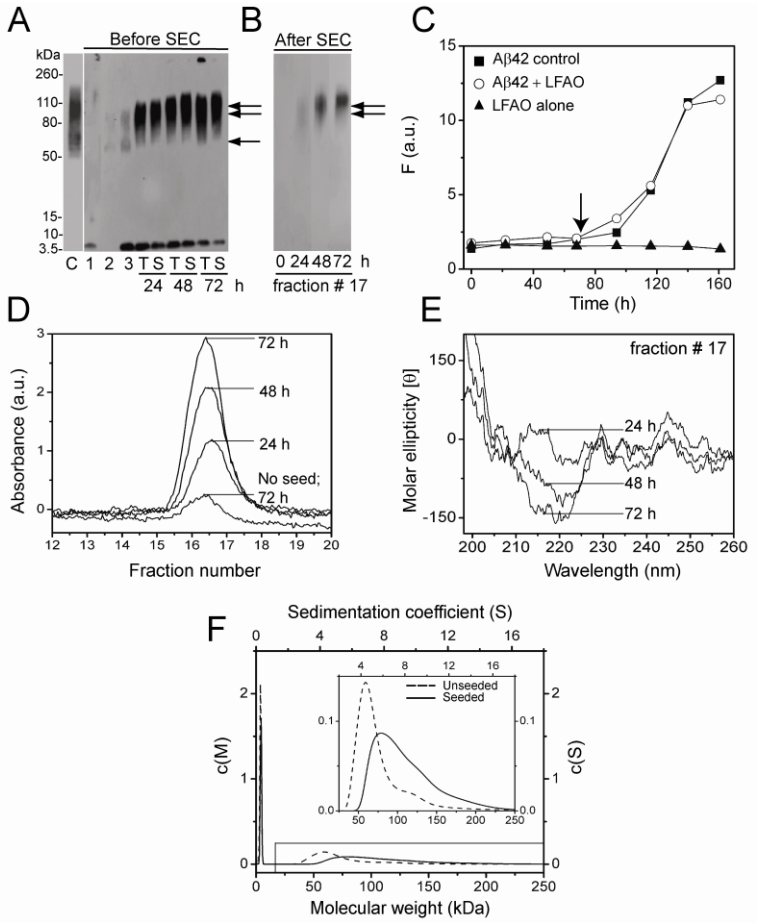

Figure 17. LFAOs Propagate upon Interacting with Monomers. A) Immunoblot of 20 μM Aβ42 incubated with 0.4 μM LFAO (2 % seed) for 72 hours at room temperature before and after SEC. C represents LFAO control (338 ng). Lanes 1 and 2 are Aβ42 control after 72 hours in the absence of LFAO seed and LFAO alone (28 ng), respectively. Lane 3 is an aliquot of 20 μM Aβ42 seeded with 0.4 μM LFAO immediately after incubation (0 h). Lanes T and S represent the total and supernatant of the sample after centrifugation at 19,000 x *g* for 20 min, at the indicated times of incubation. The volume of sample loaded was kept constant to ensure 28 ng of the parent LFAO was maintained. B) Immunoblot of fraction 17, fractionated by SEC after 24, 48 & 72 hours of incubation of the samples in A (lanes S). C) ThT fluorescence data of the seeded reaction. The arrow indicates the 72 hour point to which the seeding reaction was monitored. D) Fraction 17 of the seeded samples, which was fractioned on a Superdex-75 column after 24, 48 & 72 hours along with a control sample (no seed) after 72 hours. E) The corresponding far-UV CD spectra of fraction 17, and F) Normalized relative molecular weight distributions, *c(M)* profiles obtained from sedimentation velocity data for control LFAOs (dotted line) and seeded oligomers (smooth line). (Inset) Expanded region of the *c(M)* plot indicated in the figure.

Morphology of propagating LFAOs

The morphology of the seeded sample was also monitored using AFM at different time points to observe any changes that might occur during propagation (Figure 18). The 0 hour sample, i.e. immediately after seeding (Figure 18A & D), showed few spherical, small, punctate dots ~8 nm in heights, representing LFAOs. The 48 hour (Figure 18B & E) sample showed a considerable increase in the number of spherical LFAOs along with a slight increase in height (~12 nm), and they appear to align in a straight linear line (*inset*). The sample after 72 hours (Figure 18C & F) showed a further increase in the number of spherical dots with similar height profiles (~14 nm), along with a linear alignment of the particles (*inset*) and a few smooth fibrillar structures. More importantly, the linear alignment of these spherical particles gives the overall appearance of 'maturing' PF. A similar type of linear arrangement was observed previously when Aβ40 was incubated in the presence of aqueous-organic interface.[93] Furthermore, AFM data complements the immunoblotting and AUC data and suggests that LFAO undergoes propagation.

Incorporation of Monomers into Replicated LFAOs

N-terminal Dansyl labeled Aβ42 (Dan-Aβ42) was used as a fluorescent probe to further ensure that seeding leads to incorporation of monomers into replicated LFAOs assembly.

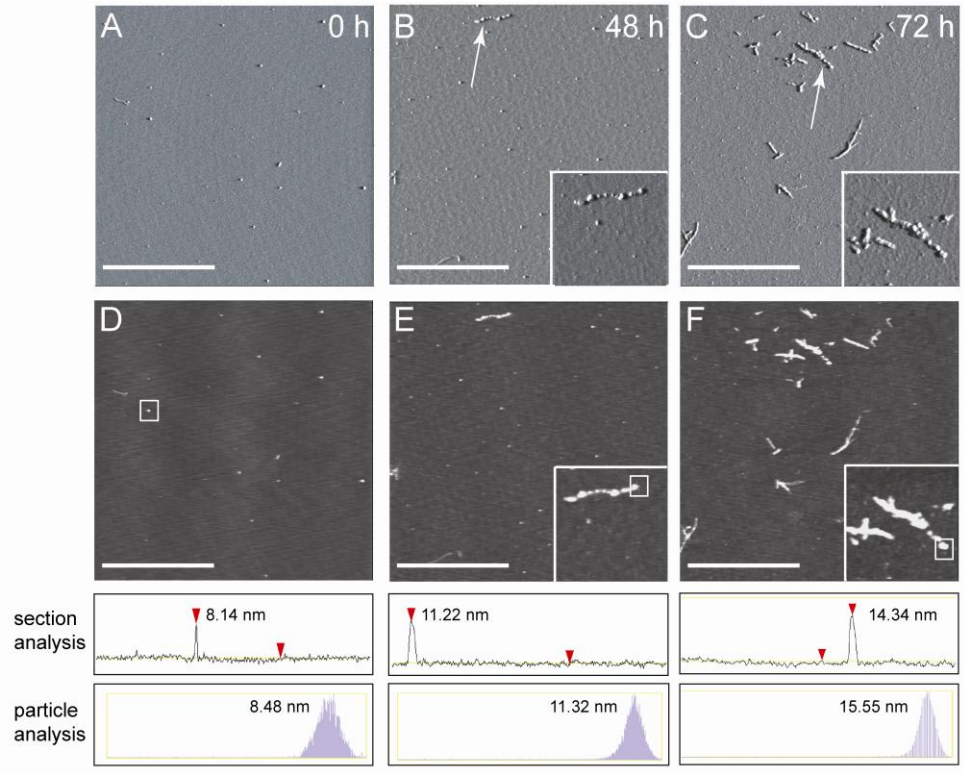

Figure 18. Morphological Changes during LFAO Propagation. Aliquots of the samples from Figure 17A (before SEC) were probed at different time points to see the propagation of oligomers after incubating 20 μM Aβ42 with 0.4 μM LFAO (2 % seed) for 72 hours at room temperature. A, B & C, represent AFM images of the seeded sample after 0, 48 & 72 hours, respectively (z scale, 0-0.8 V). D, E, and F represent the corresponding height data from A, B & C, respectively (z scale, 0-40 nm). The white scale bar represents 2.5 μm, and the inset shows a field of dimensions 1 x 1 μm surrounding the particles indicated with arrows. The white boxes in D-F indicate the particles for which the height analyses were conducted. Height profiles were extracted from the flattened height data and can be seen from the z direction in the height images and from the x, y direction below each image. These height profiles demonstrate how approximate feature heights were determined for each sample. The determined feature heights were confirmed via particle analysis (Nanoscope version 5.30 r2 image analysis software), shown at the bottom as a secondary technique to increase confidence in reported values.

A schematic of the reaction of Dan-Aβ42 and LFAOs is shown in Figure 19A, indicating that seeding with LFAO should generate replicated oligomers containing labeled peptides, which can be easily detected by intrinsic fluorescence. A seeding experiment similar to Figure 17A was performed using 50 μM Dan-Aβ42 and 1 μM

LFAOs for 72 hours at room temperature. After 72 hours, the seeded sample was centrifuged at 19,000 x *g* to remove any fibrils, and the supernatant was subjected to SEC fractionation and immunoblotting (Figure 19B & C). The SEC profile for the isolation of propagated LFAOs was exactly comparable to the isolation profile in Figure 17D. The immunoblot also clearly showed a significant increase in the amount of LFAOs after 72 hours as compared to 0 hour (Figure 19C, lanes 4, 5, & 6). The SEC fractionated sample (fractions 17 & 18) also showed the presence of replicated LFAOs in immunoblot (Figure 19C, lanes 8 & 9), whereas monomers were fractionated in the inclusion volume peak at fraction 24 (Figure 19C, lanes 10). The fluorescence spectra of fractions 17 & 18 were collected by exciting the sample at 350 nm while monitoring Dan-Aβ42 emission at 450 nm (Figure 19D). Importantly, both fractions showed dansyl emission at 450 nm, indicating that Dan-Aβ42 monomers were incorporated into the propagated LFAO assembly upon seeding, providing an unambiguous confirmation for the replication mechanism. In sum, the collective data suggest that LFAOs are self-propagating strains of Aβ oligomers.

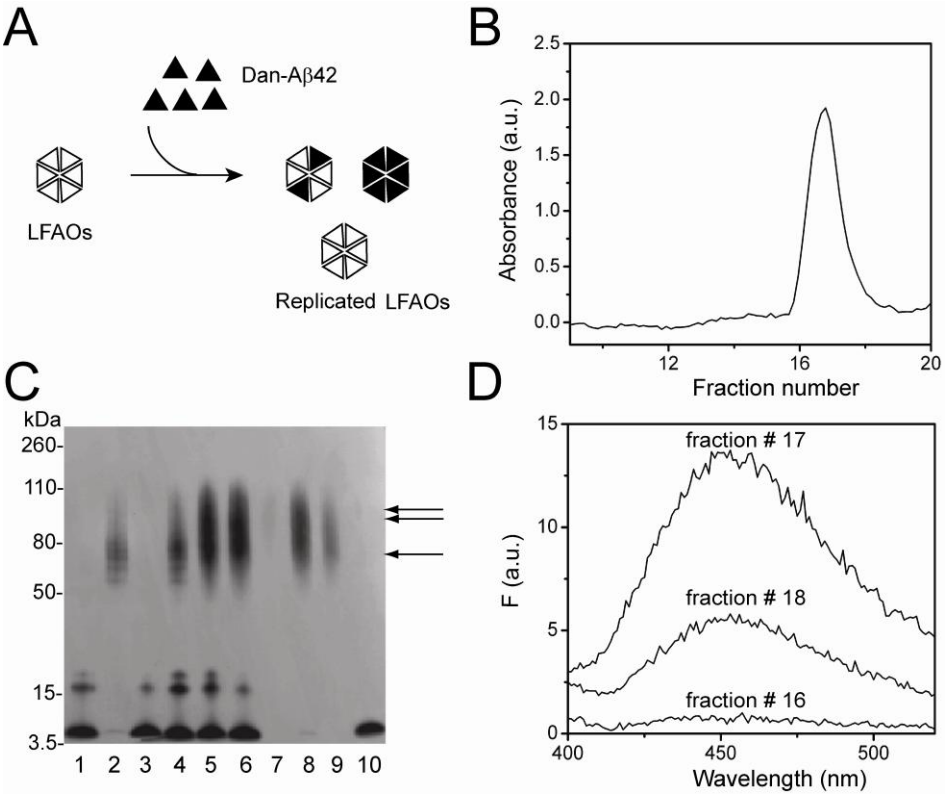

Figure 19. Incorporation of Dan-Aβ42 Monomer into Replicated Oligomers after Seeding. A) Schematic for incorporation of Dan-Aβ42 into propagated LFAOs after seeding for 72 hours. B) 20 μM Dan-Aβ42 incubated with 0.4 μM LFAO (2% seed) for 72 hours at room temperature. The seeded sample was fractioned on a Superdex-75 SEC after 72 hours; Inset – immunoblot showing the comparison of seeded sample before and after SEC. C represents control LFAO (338 ng). Lane 1 shows Dan-Aβ42 control after 72 hours. Lane 2 shows an aliquot of the sample after 0 hour (total). Lane 3 shows the incubation after 72 hours. Lanes 4 and 5 show fractionated samples, fractions 17 & 18, respectively, after 72 hours. C) Fractionated sample, fractions 17 & 18 showing the Dan-Aβ42 emission at 450 nm upon exciting at 350 nm with a band width of 20 nm (10/10).

LFAOs Form Non-fibrillar, Diffuse Aggregates in Aqueous-Organic Phase Interfaces

buffer-hexane and buffer-chloroform experiments. Interfaces are well known to affect Aβ aggregation, especially aqueous-organic phases.[47] It has been recently shown that prefibrillar oligomers (PFOs) form distinct pore like structures called annular protofibrils (APFs) upon interaction with water-hexane interfaces, which remain stable for long periods of time without forming fibrils.[47] It is believed that the formation of this

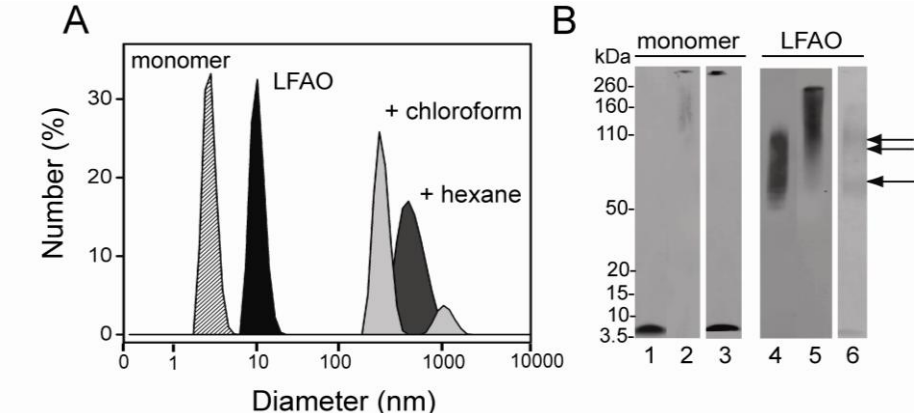

Figure 20. LFAO Agitation in Interfacial Environments. A) The increase in size of LFAO after agitation with 5% (v/v) hexane or chloroform in buffer followed by dialysis for 23 hours was monitored by DLS. B) Immunoblot of the agitation experiments along with monomer controls. Lane 1 shows control monomer Aβ42; lanes 2 and 3 dialyzed 23 hours Aβ42 monomer sample treated with chloroform & hexane, respectively. Lane 4 shows control LFAO; lanes 5 and 6, dialyzed 23 hour Aβ42 sample treated with chloroform & hexane, respectively. The single and double arrows indicate 50-70- and 80-110-kDa bands, respectively.

ring/pore like structures is one of the mechanisms by which oligomers exert their toxicity. The effect of aqueous-organic phase interfaces on LFAOs was explored to observe whether they could form any non-fibrillar off-pathway aggregates like APFs. Two interfacial systems were used for these experiments: hexane-water (as used previously for PFOs) and chloroform-water. For this experiment, a protocol previously published for PFOs was followed, and based on that protocol, freshly isolated 2 μM LFAOs were

mixed and agitated with 5% (v/v) hexane-water on a vortexer for 1 hour.[47] After agitation, the sample was dialyzed at room temperature for 23 hours, followed by DLS analysis of the dialyzed sample. The LFAOs treated in hexane-water prominently exhibited the formation of large species with a hydrodynamic radius of ~700 nm (Figure 20A, gray peak), whereas LFAOs in buffer alone showed a monodisperse peak with a ~10 nm diameter (Figure 20A, black peak) correlating well with the AFM data (Figure 15A, inset), which showed an average height range of 7-10 nm. But an immunoblot of the same sample failed to show any large species; instead an unexpected decrease in the band intensity was observed (Figure 20B, lane 6). Interestingly, upon the same treatment, Aβ42 monomer showed a high molecular weight species band that failed to enter the gel, indicating the formation of fibrils (Figure 20B, lane 3).

The same experiment was repeated with the chloroform-water system, to see whether it was possible to replicate the formation of larger aggregates in other interfaces too. The main advantage of using chloroform as compared to hexane is that it is denser than water, and buffers can be easily suspended at the top of the organic layer. The 2 μM LFAOs were mixed, agitated and dialyzed in a similar manner as with hexane and monitored by DLS, which showed a polydisperse distribution of species with two peaks: ~700 and 1000 nm (Figure 20A, light gray peak). The immunoblot of the dialyzed sample showed a significant shift towards a higher molecular weight band, further complementing the DLS data (Figure 20B, lane 5). In contrast, upon the same treatment, Aβ42 monomer again showed the formation of a very large molecular weight species that failed to enter the gel (Figure 20B, lane 2).

morphology of the aggregates formed after chloroform and hexane treatment. The AFM image of the LFAO treated with hexane-water interface showed the presence of very large spheroidal aggregates with an average height of ~33 nm (Figure 21 A). The spheroidal aggregates were almost 3-4 times larger than individual LFAOs in apparent diameter and are believed to result from association of LFAOs (Figure 21A). In contrast, Aβ42 monomer treated with hexane showed the presence of fibrillar structures (Figure 21B). It is important to point out that LFAOs do not form any ring- or pore-like structure like PFOs on hexane treatment, indicating that the assembly of different soluble oligomers can vary depending upon their molecular organization.[47] LFAOs treated with chloroform also showed the presence of large aggregates with an average height of ~21 nm (Figure 21C). More importantly, Aβ42 monomer treated with chloroform does not show any large fibrillar structures (Figure 21D), as expected based on the immunoblot data that clearly indicate the presence of a high molecular weight band at the top of the gel (Figure 20B, lane 3). It is possible that dilution during AFM sample preparation might have caused the disaggregation of unstable aggregates formed in chloroform interfaces. This observation was similar to the report published previously for Aβ40, in which unstable aggregates get completely disaggregated upon dilution.[52] Collectively, DLS and AFM data indicate that LFAOs, upon treatment with interfaces, also form large, non-fibrillar, disperse aggregates with completely different morphology from PFOs and that these aggregates may not be the intermediates of the fibril formation on-pathway.

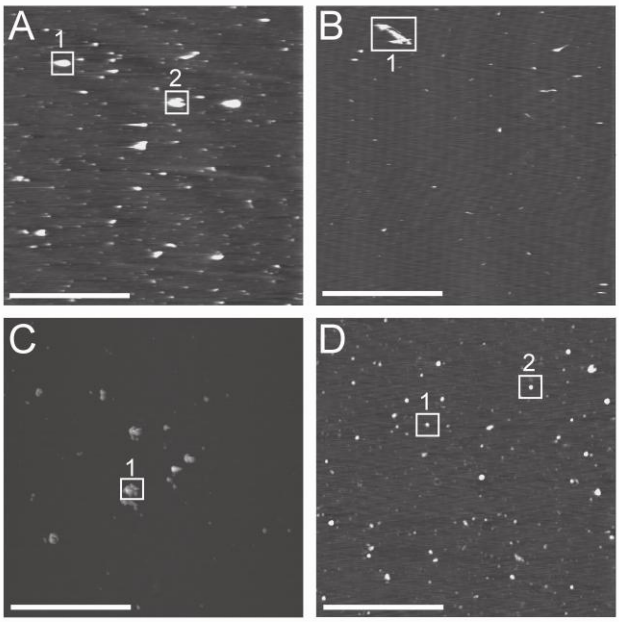

	sample	section analyses (nm)		particle analyses (nm)	
		1	2	1	2
A	LFAO + hexane	35.66	33.25	37.44	36.96
B	monomer + hexane	11.10	—	—	—
C	LFAO + chloroform	21.50	—	—	—
D	monomer + chlorofrom	8.57	10.57	9.31	10.96

Figure 21. Morphology of Aggregates Formed after Treatment with Chloroform and Hexane. A & B) AFM images of LFAO and monomer Aβ42 control, respectively, agitated with hexane. A) LFAOs show the presence of small globular aggregates and large clumps of aggregates. B) Control monomers treated with hexane show the presence of fibrils. C & D) AFM images of LFAO and monomer Aβ42 control, respectively, agitated with chloroform. C) LFAOs show the presence of several large clumps of aggregates. D) Control monomers treated with chloroform failed to show the presence of any aggregates. The height images are presented here. The white scale bar represents 2.5 μm, and the inset shows a field of dimensions 1 x 1 μm surrounding the particles indicated in the box. The z scale for all the images is 0-40 nm. These height profiles demonstrate how approximate feature heights were determined for each sample. The determined feature heights were confirmed via particle analysis (Nanoscope version 5.30 r2 image analysis software) shown at the bottom as a secondary technique to increase confidence in reported values.

Discussion

The physiochemical properties of LFAOs that were characterized in this section indicate that they are diffuse oligomeric species with a molecular mass ranging from ~56-110 kDa. More importantly, immunoblots of isolated LFAOs showed two prominent band distributions: a lower molecular weight species band ranging from ~56-70 kDa and a high molecular weight species band from ~ 80-110 kDa, corresponding to 12-15mers and 18-24mers respectively. AUC sedimentation velocity data complemented the observation that LFAOs are a mixture of oligomeric species, with a heterogeneous peak distribution of species corresponding to 5 S, and 7-12 S sedimentation coefficients. A somewhat similar AUC sedimentation velocity profile was recently published by Freir and coworkers for ADDLs, indicating that they are also a heterogeneous mixture of oligomeric species larger than 90 kDa with a very disperse c(S) distribution ranging from 10 S to 25 S.[108]

The most significant and novel property of LFAOs is their *self-propagation* behavior, which can help discover new insights into the pathogenesis of AD. The LFAOs can act as seeds to convert non-toxic monomers into toxic, non-fibrillar aggregates, displaying a mechanism similar to the 'template-assisted corruptive' self-propagation of prion proteins (Figure 22A).[77, 109, 110, 111] It is also possible that the self-propagation of LFAOs can act as a *trap* to direct more monomers away from the fibril formation on-pathway to a more toxic off-pathway. Furthermore, propagation leads to a quantitative increase in the amounts of LFAOs formed. The key practical utility of this property is that it could be exploited to enhance the amount of endogenous oligomeric seeds by amplification to an extent amenable for biophysical characterization, following a method

similar to the 'Protein Misfolding Cyclic Amplification (PMCA)' method reported previously by Soto and co-workers for *in vitro* prion protein amplification (discussed in the next section).[78, 112]

LFAO: A Novel Off-pathway Self-propagating Intermediate

All the data presented so far further support our proposed hypothesis that oligomers need not be formed along the mandatory fibril formation pathway. LFAOs and some other oligomers, like PFOs and FOs, share a common trait in that all of them nucleate the formation of oligomers from monomers but not fibrils.[47, 86, 113] Furthermore, the formation of non-fibrillar aggregates upon interactions with monomers and also on LFAOs association suggest that the LFAOs are off-pathway intermediates that can also compete and recruit more monomers towards this toxic pathway through a unique replication mechanism (Figure 22B). More importantly, the association property of LFAOs upon their interfacial interaction can provide valuable insights about the mechanism and behavior of endogenous LMW oligomers in the presence of lipid interfaces in the physiological environment. Figure 22B also illustrates the possibility of energy minimum states along the aggregation pathway, and it is likely that oligomers get trapped in these kinetic minima and thereby promote prolonged toxicity. Therefore, it is possible that these off-pathway routes can recruit more monomers to populate LMW oligomers and are more toxic than the nucleation dependent on-pathway.

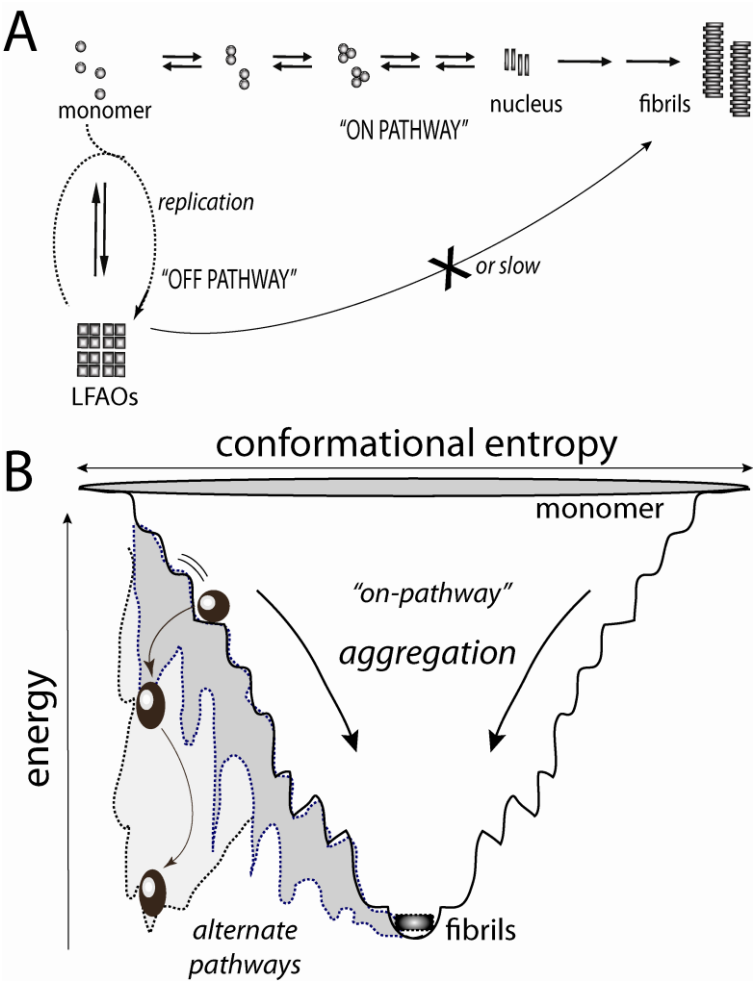

Figure 22: Schematic Diagram Depicting the Generation of 'Off-pathway' Oligomers and Propagation. A) The classical fibril formation 'on-pathway' of Aβ aggregation along with an 'off-pathway' is depicted. The process of replication of off-pathway oligomers is shown with dotted lines. B) An aggregation funnel is similar to the protein folding funnel but depicts the aggregation of intrinsically disordered proteins such as Aβ towards fibril formation. This path is considered the nucleation-dependant 'on-pathway'. The spherical balls represent LMW oligomers. However, it is possible that the oligomers adopt a different pathway such that they are trapped in local energy minima as 'off-pathway' species (oval ball; grey area of the funnel). Such off-pathway species would have a significant energy barrier to overcome in order to proceed towards fibrils. Also, the off-pathway oligomers could recruit more monomers and dictate them to adopt such pathways (replication process). This may further increase the energy barrier for such off-pathway oligomers to overcome and significantly increase their half-lives in doing so.

Evaluation of Prion-type Behavior of LFAOs

Encouraged by the prion-like template assisted self-propagation mechanism displayed by LFAOs as described in the previous chapter, we wanted to further explore whether LFAOs are indeed 'Prions'.[112, 114] The scrapie form of prion, PrP^{Sc} (misfolded prion protein), is known to undergo a 'protein misfolding cyclic amplification' (PMCA) process in which small amounts of PrP^{Sc} seeds can be amplified upon making them interact with the folded, non-toxic form (PrP^{C}) of the protein under controlled conditions *in vitro*.[112, 114] Such *in vitro* amplified prions are reported to retain the infectious properties of their *in vivo* counterparts.[115] The utility of PMCA is that the assay can be used as a diagnostic tool for detecting the presence of pathogenic prions by amplifying extremely low amounts of *in vivo* PrP^{Sc} seeds. The amplification of seeds by the *in vitro* PMCA assay is greatly influenced by the parameters like buffer, temperature, pH, sonication and time of incubation etc.[112, 114] Therefore, for LFAO self propagation, optimization of some these crucial parameters is essential to see how, if at all, they can affect the propagation efficiency of LFAOs.

Cyclic Propagation of LFAOs

In order to assess whether LFAOs could undergo PMCA-type amplification as reported for prions, the PMCA protocol developed by Soto and colleagues was followed for the amplification of LFAOs, with some modifications.[114-116] It is interesting to point out that LFAOs showed self-propagation behavior at an ambient temperature without requiring any special sonication conditions, which is critical for *in vitro* prion amplification.[112, 114]

First, as described in the previous section, LFAOs were subjected to self-propagation by seeding (2%) 50 μM buffered Aβ42 monomers at room temperature for 72 hours. After 72 hours, the incubated sample was centrifuged at 19,000 x *g* for 20 min to remove any fibrils, and the supernatant was subjected to fractionation by SEC using a Superdex-75 column (Figure 23A). This amplification/propagation cycle of LFAO was termed as 'Cycle-1'. The comparison of SEC profiles of the seed alone (dotted line) and seeded sample (black line) are shown in Figure 23A. The seeded sample showed a ~3.5 fold increase in the amount of seeds after Cycle-1 as compared to seed alone (Figure 23D; Cycle-1), consistent with our previous observation (Chapter IV.2). The immunoblot of the aliquots of seeded sample (Figure 23 E; Cycle-1, lanes T&S) after 72 hours prior to SEC also showed a similar increase in the amount of LFAOs compared to seed alone (Figure 23 E; lane seed). More importantly, the seeded sample (Figure 23E; Cycle-1, lanes T&S) showed a replicated LFAO (R-LFAO) band centered around ~100 kDa after Cycle-1, which was also consistent with our previous observation that replication led to the formation of higher molecular weight species of LFAO (~80-110 kDa) (Chapter IV.2; Figure 17).[113] SEC fractions 16 and 17 (Figure 23 E; Cycle-1, lanes 1&2) also showed the presence of isolated R-LFAOs. Moreover, a high molecular weight band, which failed to enter the gel and was likely fibrils, was also observed after 72 hours in seeded samples (Figure 23 E; Cycle-1, lane T).

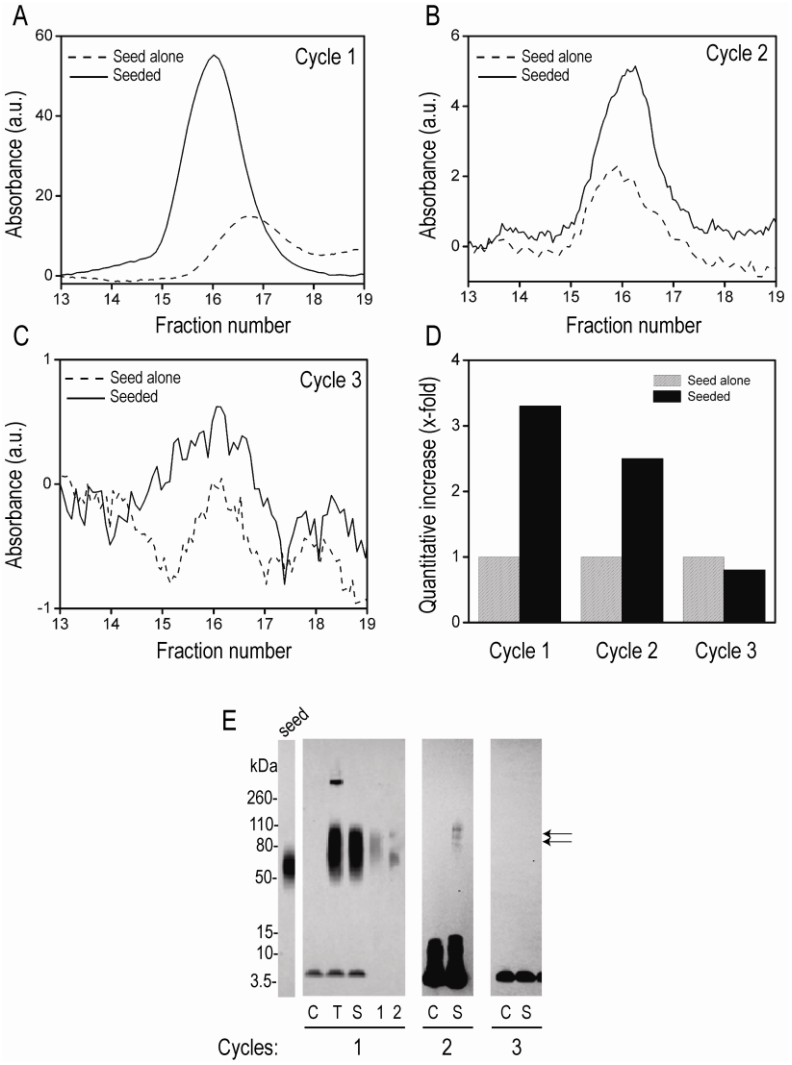

Figure 23. Cyclic Propagation of LFAOs. A, B & C show LFAO propagation cycles after 72, 96 and 212 hours, respectively, monitored by SEC fractionation on a Superdex 75 column. The SEC profile comparison of seeded sample (solid line) with seed alone (dotted line) was shown to indicate the quantitative increase in the amount of LFAOs after each cycle. D) The quantitative estimate of LFAOs' fold increase after each cycle was calculated by comparing the SEC peaks of seeded with seed alone. E) Immunoblot of LFAO samples after each amplification cycle. Lane seed shows the LFAO used as seed for cycle 1. Lane C shows an Aβ42 control without any seeds for each cycle at indicated time points. Lanes T & S show the total and supernatant of the seeded sample after centrifugation at 19,000 x *g* to remove any fibrils after each amplification cycle. Lanes 1 & 2 shows replicated LFAOs in SEC fractions 16 & 17 after Cycle-1.

The fibril band was absent in the supernatant (Figure 23E; Cycle-1, lane S), further confirming that these bands were indeed fibrils. The presence of some fibrils is expected due to on-pathway fibril formation reactions (monomer-monomer interactions) that occur simultaneously to monomer-LFAO interactions. For the second propagation cycle (Cycle-2), the SEC fractionated R-LFAOs from Cycle-1 (fraction 16, lane 1; Figure 23 E) were used as seeds (50% v/v) to 50 μM Aβ42 monomers at room temperature for 96 hours (Figure 23 B). A 50% v/v was used for seeding in Cycle-2 because the precise concentration of isolated R-LFAOs was difficult to calculate due to dilution. After several screens, we increased the incubation time from 72 to 96 hours for Cycle-2, because the amount of seeds used were approximately 2/3 less than in Cycle-1. After 96 h, the supernatant of the seeded sample was subjected to SEC fractionation, and fractions 16 and 17 were collected and compared to the seed alone (Figure 23 B; Cycle-2). The seeded sample in Cycle-2 showed a ~2.3 fold increase after 96 hours (Figure 23D; Cycle-2). Interestingly, the seed alone showed a faint R-LFAO band centered around ~ 100 kDa (Figure 23 E; Cycle-2, lane S), but fractionation did not lead to detectable amounts on immunoblot (data not shown). The amplification cycle was further continued using fraction 16 of Cycle-2 as seed (50% v/v), but the incubation time was increased to 212 hours in order to be able detect the replicated oligomers. No amplicafication was observed even after 212 hours (Figure 23 D; Cycle-3). As expected, the corresponding immunoblot did not show the presence of any R-LFAOs (Figure 23 E; Cycle-3, lane S). Based on the SEC profiles, the concentrations of seed used in Cycles -2 & -3 were approximately estimated to be around 0.29 μM (0.59%) and 0.025 μM (0.05%) respectively (data not shown).

The data clearly indicates that LFAOs undergo significant amplification after Cycle-1, but amplification efficiency decreases by ~35% after Cycle-2 and becomes insignificant after Cycle-3. There could be two possible reasons for this behavior: *a*) R-LFAOs are less efficient in amplification because of their larger size as compared to original LFAOs (~100 kDa versus 56-80 kDa for LFAOs and R-LFAOs respectively). A similar observation was reported for PrP^{Sc} protein by Castilla *et al.*, in which they showed that larger aggregates of PrP^{Sc} formed above 100 °C are less efficient for amplification as compared to parent PrP^{Sc}.[115] *b*) The amount of seeds used in Cycle-3 is well below the threshold concentration of seed (minimum amount required to self-propagate).[101, 117]

Comparison of Seeding Efficiency of R-LFAOs vs. Parent LFAOs

First we wanted to analyze the effect of size difference between LFAOs and R-LFAOs on self-propagation. Cycle-2 of LFAO amplification, in which R-LFAO, the larger oligomeric band (~80-110 kDa) of native LFAOs, was used as a seed, showed less efficient propagation as compared to Cycle-1, which used parent LFAOs (~56-80 kDa). The R-LFAOs were generated as previously described (see Materials & Methods). In order to see whether larger aggregates are less efficient in promoting amplification, the same LFAO propagation procedure was repeated using 2% of SEC isolated R-LFAOs as seed for 20 μM buffered Aβ42 monomer. The same percentage of original LFAO seed was also used as a control for the comparison of propagation efficiency with R-LFAOs. After 96 hours, both samples were subjected to immunoblotting and SEC. Additionally, to keep the conditions of the amplification cycle constant, samples were incubated for 96 hours instead of 72 hours. In Figure 24 (inset), lanes 2 and 4 show the control and R-LFAOs samples after 96 hours respectively. The immunoblot band intensity for both the

samples was identical. However, quantitative SEC comparison showed a ~2.4 and ~1.6 fold increase for the control and R-LFAO seeded sample, respectively (Figure 24). More interestingly, R-LFAOs showed a ~33 % decrease in amplification efficiency as compared to control, which is identical (~35 %) to the decrease observed after Cycle-2 of LFAO amplification (Figure 32). The data clearly indicates that larger ~80-110 kDa R-LFAOs are less efficient in amplification as compared to native LFAOs, further complementing our previous observation.

Physiochemical Differences and Similarities between LFAOs and Prions

effect of temperature on LFAO propagation and other physiochemical properties.

Previous studies on PrP^{Sc} protein replication and propagation have shown that high temperatures can promote the formation of larger aggregates, which can greatly reduce the amplification efficiency.[115] To investigate whether LFAOs showed a similar property, the effect of temperature on LFAO propagation was explored. A 7 μM incubation of LFAOs was heated for 5 min at specific temperatures ranging between 10 and 120 ^{o}C and subjected to DLS analysis. Small aliquots of these samples were then subjected to immunoblotting (Figure 25A). A significant shift towards higher molecular weight was observed for samples heated at 80, 100 and 120 °C (Figure 25A, lanes 2, 3, & 4) as compared to control unheated LFAOs (Figure 25A, lane 1). The 100 and 120 °C samples showed a large disperse band ranging from 80 to >260 kDa.

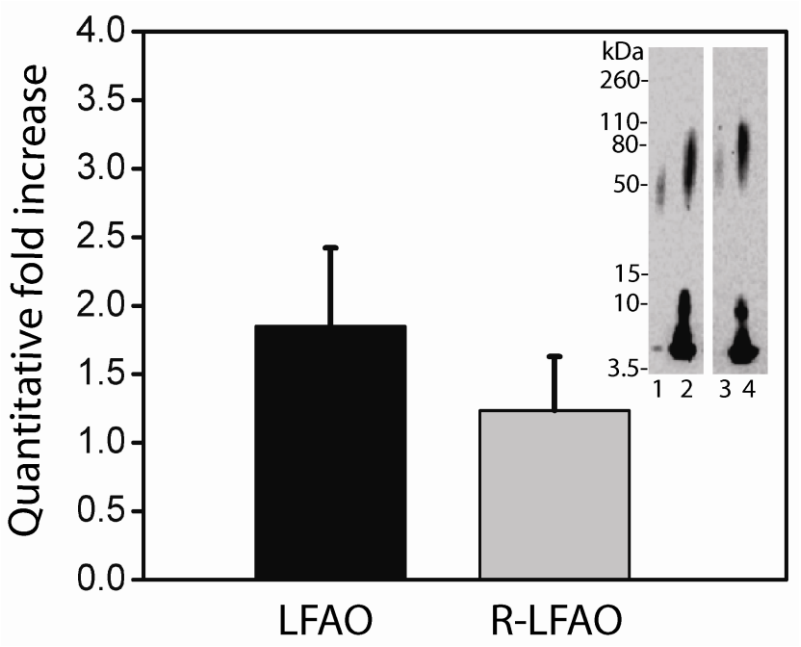

Figure 24. Comparison of Propagation Efficiency of Parent LFAO vs. R-LFAO. 20 μM Aβ42 was incubated with 2% (molar ratio) parent LFAO (black bar) and replicated LFAO (R-LFAO, grey bar) at room temperature for 96 hours. After 96 hours both the samples were subjected to SEC and quantitative fold increase was calculated by comparing the SEC profiles. The inset shows an immunoblot of LFAO and R-LFAO seeded sample after 96 hours. Lanes 1 & 2 shows parent LFAO seed alone and 96 hour seeded sample, respectively. Lanes 3 & 4 shows R-LFAO seed alone and 96 hours seeded sample, respectively.

A similar shift towards larger size was also observed for 80, 100 and 120 °C samples in DLS (Figure 25 B). The heat-treated LFAO samples at 80 (dark grey), 100 (grey) and 120 °C (light grey) showed monodisperse peaks centered at ~11 , ~18 and ~ 37 nm in diameter, respectively, all of which were larger in diameter than the unheated LFAO sample (black peak; ~7 nm in diameter) (Figure 25B). It is evident that an increase in temperature promotes larger aggregates of LFAOs. The treatment of LFAOs at lower temperatures (20-60 ^{o}C) did not cause any changes compared to the unheated LFAO sample in either DLS or immunoblots (data not shown). The CD analysis showed

an increase in β-sheet content, characterized by a minimum at 216 nm, with increasing temperature (Figure 25 C). This observation was consistent with the report by Gursky and colleagues, who showed that heating Aβ40 at higher temperatures caused an increase in β-sheet content, suggesting further oligomerization and aggregation.[118] Similar reports have also been reported for other amyloidogenic proteins.[119]

Next, we compared the seeding and propagation efficiency of 80, 100, and 120 °C heated LFAO sample with unheated LFAO sample. For seeding and propagation, 20 μM freshly purified, seed-free Aβ42 was incubated at room temperature for 72 hours either with 0.4 μM (2% molar ratio) unheated LFAO as a control or with LFAOs that had previously been heated to 80, 100 or 120 °C. Immunoblot lanes 2, 4, 6, and 8 show the comparison of propagation efficiency between unheated and 80 and 100 °C heated LFAO samples (Figure 25 D). The quantitative fold increase, determined by comparing the SEC peaks of seeded sample and seed alone, and indicated a ~2.5 fold increase for the unheated LFAO sample (Figure 25E, unheated). In contrast, the 80, 100 and 120 °C heated LFAO samples showed 1.4, 0.7 and 0.4 fold increases respectively (Figure 25 E; 80, 100, & 120 °C), indicating a decrease in amplification/propagation efficiency with the increase in temperature. A statistical analysis of variance (ANOVA) on the data indicated >90% (Figure 25 E, 80 °C; ●) and >99% (Figure 25 E, 100 & 120 °C; **) significance in the difference between the seeding efficiency of unheated LFAO and 80, 100 and 120 °C heated LFAO after 72 hours.

The data also suggest that, although they do so with diminished efficiency, even the larger aggregates of LFAO were able to undergo self-propagation, as no fibrils were observed. This clearly demonstrates that the entire propagation process occurred along

the off-pathway, as we had hypothesized (see chapter IV.2.). The data further indicates that higher temperatures can induce the formation of larger aggregates and reduce the amplification efficiency, a behavior similar to PrP^{Sc} propagation.[115]

determination of LFAOs' threshold seed concentration and seeding efficiency. A minimum critical concentration of seeds is required for the initiation of polymerization in nucleation-dependent aggregation reactions.[101, 117] In order to determine the threshold seed concentration for LFAOs to undergo self-propagation, 30 μM buffered Aβ42 was incubated with 0.2, 2, and 20% (molar ratio) LFAO seed at room temperature for 212 hours. Small aliquots of samples were removed at 72, 144 and 212 hours and subjected to SEC and immunoblotting to observe the quantitative increases in the amount of LFAOs (Figure 26).

Immunoblot lanes 1, 2, and 3 show 0.2, 2, and 20% LFAO seed alone, respectively (Figure 26 A), and lanes 4, 5, and 6 show 0.2, 2, and 20% LFAO seeded sample after 212 hours, respectively (Figure 26 A). A significant increase in the amount of LFAOs was observed in the immunoblot for the 0.2% seeded sample (Figure 26 A, lane 4), as compared to the seed alone (Figure 26 A, lane 2), which was undetectable after 212 hours. The quantitative increase in LFAOs after each time point was calculated by comparing SEC peaks of seeded sample versus seed alone (Figure 26 C). Figure 26 B represents the SEC profiles of 0.2 (continuous line), 2 (dotted line), and 20% (dashed line) seeded samples after 212 hours respectively.

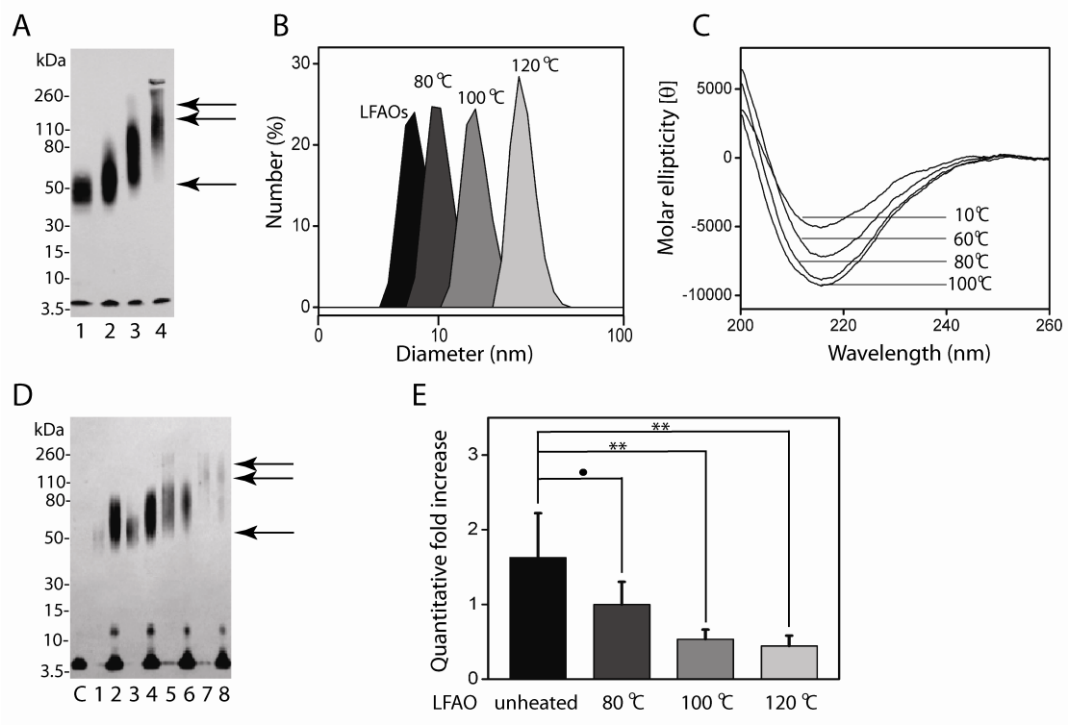

Figure 25. Effect of Temperature on LFAOs. A) Immunoblot showing LFAOs heated at different temperatures. Lane 1 shows unheated LFAO sample as a control. Lanes 2, 3, & 4 show LFAOs heated at 80, 100 and 120 °C, respectively. The increase in LFAO size after heating is shown by double arrows. B) DLS analysis of LFAOs heated at different temperatures. C) CD spectral analysis of LFAOs heated at different temperatures. D) Immunoblot showing a comparison of propagation efficiency of unheated vs. 80, 100 & 120 °C LFAOs after 72 hours. Lanes 1 and 2 show unheated LFAO seed alone and seeded sample, respectively. Lanes 3, 5 & 7 represent 80, 100 & 120 °C heated 0.4 μM (2% molar ratio) LFAO seed alone, respectively, while lanes 4, 6 & 8 represent 20 μM Aβ42 incubated with 0.4 μM (2% molar ratio) 80, 100 & 120 °C heated LFAO seeds, respectively. E) Determination of LFAOs' quantitative fold increase, determined by comparing the SEC profiles of the unheated, 80, 100 and 120 °C heated LFAO seeded samples with seed alone; ● and ** represent 90 and >99.9% significance, determined via ANOVA.

The reaction seeded with 0.2% LFAOs showed a ~6 fold increase as compared to ~2 fold increases by 2 and 20% seeded reactions after 212 hours (Figure 26 C). The 0.2% sample also showed a significant increase in LFAOs after 72 and 144 hours, but the maximum efficiency was observed only after 212 hours (Figure 26 C). Statistical

analysis on the data indicated >99.9% (Figure 26 C; ***) confidence in the increase of LFAO amount for 0.2% as compared to 2 and 20% after 212 hours. All attempts to detect LFAOs in 0.02% (molar ratio) seeded samples by SEC and immunoblots were unsuccessful (data not shown); indicating that this seed concentration was below the threshold of optimal seeding efficiency.

Collectively, the data show that 0.2% (molar ratio) LFAO is the most efficient seed concentration for promoting propagation to an exceptionally significant limit, allowing for easy detection by SEC and immunoblots. Furthermore, the data indicate that the threshold seed concentration of LFAOs required to initiate propagation for 30 μM Aβ42 is ~0.06 μM (270 ng/mL), below which replication is experimentally undetectable. The data further explain our observation that Cycle-3 of the LFAO propagation/amplification (Figure 23 C), which was initiated by 0.025 μM seed, completely failed to show any propagation, as the LFAO concentration was below the threshold concentration determined here (0.06 μM).

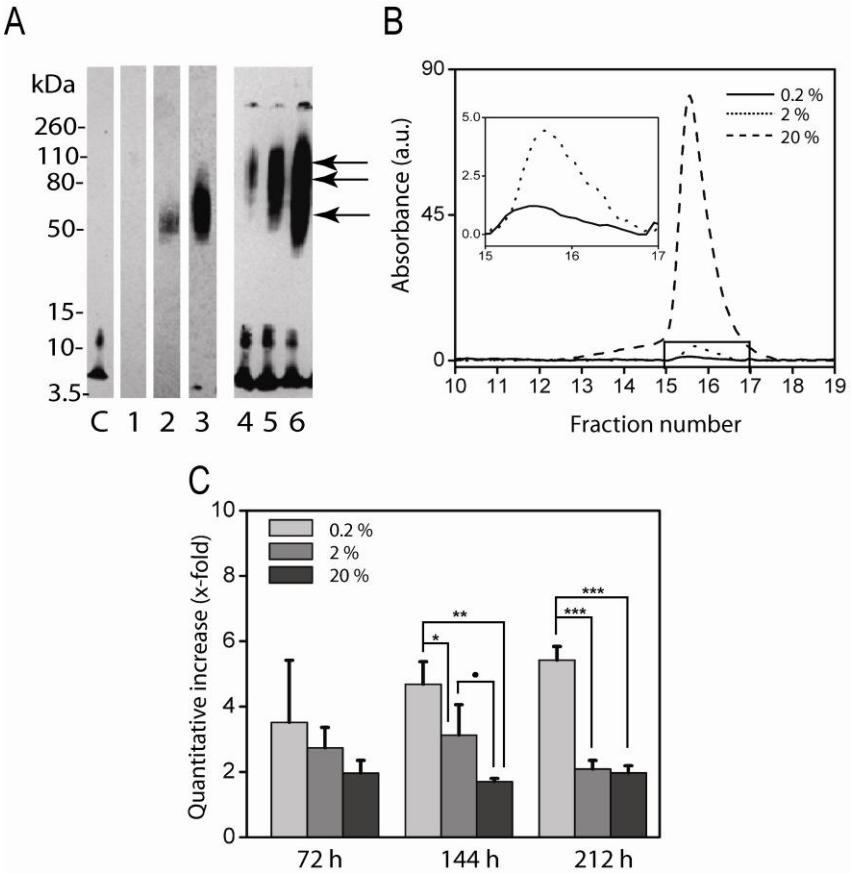

Figure 26. Determination of LFAOs' Threshold Seed Concentration and Seeding Efficiency. A) Immunoblot of 30 μM Aβ42 seeded with 0.2, 2, and 20% (molar ratio) LFAO seeds after 212 hours. Lane C shows control Aβ42 incubated alone after 212 hours. Lanes 2, 3, and 4 represent 0.2, 2, and 20% (molar ratio) LFAO seeds alone, respectively. Lanes 4, 5, and 6 represent 0.2, 2, and 20% (molar ratio) LFAO seeded sample after 212 hours, respectively. Single and double arrows indicates original LFAO seeds at ~56-70 kDa and R-LFAO bands at ~80-110 kDa after propagation, respectively. B) SEC profile of 0.2, 2, and 20% (molar ratio) LFAO seeded sample after 212 hours. C) Determination of LFAOs' quantitative fold increase at different time points, by comparing the SEC peak profiles of the 0.2, 2, and 20% (molar ratio) LFAO seeded sample with seed alone; ●, *, **, and *** represents 90, >95, >99 and >99.9% significance based on analysis of variance using ANOVA.

Discussion

In prion diseases, self propagation of the misfolded PrP^{Sc} form by a 'template-assisted corruptive' mechanism is a well known phenomenon.[77] Many recent studies on prions have shown that it is possible to replicate the *in vivo* infectious mechanism under *in vitro* conditions using the PMCA method.[112, 114, 116] In PMCA, a small amount of endogenous PrP^{Sc} seed can be amplified with complete structural faithfulness upon addition to native PrP using successive cycles of sonication and incubation to an amount easily detectable for diagnostic purposes.[112, 115]

In the AD field, prion type propagation is an emerging hypothesis, and recent *in vivo* studies have demonstrated this phenomenon in transgenic mouse models.[88] Recently, Stóhr and coworkers have shown that synthetic Aβ can act as prions and undergo self-propagation and migration upon inoculation into mouse brains.[89] In the previous results section (Chapter IV.2.), we have shown that LFAOs can also self-propagate by converting monomers into more LFAOs at the expense of fibrils, displaying a behavior similar to prions, which forms the first such *in vitro* observation.[113]

Similarity between LFAO and Prion Propagation

In this section, we have presented the similarities and dissimilarities between prion and LFAOs propagation. A method similar to PMCA was used for LFAO propagation and indicated that small amounts of LFAOs, upon monomer addition, undergo significant amplification/propagation like prions during Cycle-1, but amplification/propagation efficiency decrease by ~32% for Cycle-2, due to the formation of R-LFAOs. Propagation becomes insignificant after Cycle-3. Interestingly, the R-LFAOs, when used as a seeds for the propagation experiment also showed a ~32 %

decrease in amplification efficiency as compared original LFAO seed, clearly indicating that the higher molecular band of LFAOs is less efficient in promoting propagation. Interestingly, LFAOs, when subjected to higher temperatures, showed the formation of larger aggregates, which are less efficient in promoting amplification when used as a seed, a behavior similar to prions.[115] More importantly, data clearly indicated a similarity in the propagation behavior of LFAOs and prions in *in vitro*. LFAO propagation has an advantage in that it is very straight forward, not requiring optimization of any special parameters as in the PMCA method of prion amplification.

LFAO Threshold Seed Concentration

We could not detect any amplification of LFAOs after Cycle-3, which could be due to the seed amount being well below the threshold concentration necessary to initiate such a process.[101, 117] Seed concentrations below 0.2% failed to show any propagation efficiency and were completely undetectable under experimental conditions. Based on this analysis, the LFAO threshold seeding concentration was determined to be ~60 nM for 30 μM Aβ42 , which is 2.5 times less than the ~150 nM required to initiate *in vitro* propagation of prions.[117]

Significance

These findings are significant as they are the first comprehensive demonstration of *in vitro* prion type propagation of Aβ oligomers. So far, LFAOs are the only biophysically characterized *in vitro* oligomers that act as 'prions'. This Aβ prion propagation has immense practical implications and can be utilized to amplify small amounts of endogenous seed to amounts feasible for biophysical and structural characterization using exogenous monomers. The early detection of similar, self-

propagating oligomeric species, having similar conformation as LFAOs, in plasma and CSF could be used as a potential biomarker for diagnostic purposes in AD. Future studies will be directed towards elucidating LFAOs prion type propagation behavior in *in vivo* conditions.

CHAPTER V

CONCLUSIONS AND FUTURE WORK

Conclusion-1: All Oligomeric Species Need not Be Formed along the Obligatory On-pathway: Physiological Significance

LMW oligomers are believed to be the primary toxic species involved in the etiology of AD. As a result of their increased significance in AD pathology and lack of structural information about these oligomers, many research groups have shifted their primary focus to the identification and characterization of both *in vivo* and *in vitro* Aβ oligomers. This focused approach towards oligomers resulted in several new important findings. So far, it has been believed that oligomers are formed as transient intermediates during the fibril formation on-pathway. However, the observation of polymorphism among Aβ aggregates indicated the possibility of multiple Aβ aggregation pathways. Only a few observations have been reported indicating that Aβ oligomers may formed along an alternate pathway completely different from classical nucleation-dependent on-pathway. [41, 46, 75, 96, 120]

The significance of understanding multiple pathways lies in the fact that if some oligomers are formed along the off-pathway, they might have a longer self half-life compared to the on-pathway species, resulting in prolonged toxicity to neuronal cells. The data presented here further strengthen the multiple pathways hypotheses and indicate that both CMC as well as Aβ:fatty acid/lipid ratios play significant roles in dictating the pathway of Aβ aggregation and forming off-pathway oligomers (Chapter IV.1). Interestingly, these off-pathway oligomers seem to possess unique physiochemical properties compared to their on-pathway counterparts.

The Aβ peptide is amphipathic in nature, as result of which it has high affinity for membranes, which have in turn also been shown to affect the early stages of Aβ aggregation.[69-71, 121, 122] GM-1 gangliosides containing lipid rafts as well anionic phospholipids have also been shown to increase the rate of Aβ aggregation.[72, 123-126] Apart from lipids, oligomers generated by fatty acids like lauric acid, oleic acid and arachidonic acids were shown to inhibit hippocampal LTP in Tg2576 mice model.[37] Interestingly, other amyloidogenic proteins like α-synuclein, apolipoprotein C-II and prions have also been shown to display unique behavior in the presence of various interfaces.[127-130] Recently, it was shown that the misfolded, infectious PrP^{Sc} form of prion protein obtained from the conversion of normal, bacterially expressed, recombinant prion protein undergoes propagation only after interacting with a membrane anionic phosphatidyl surface.[131] All of the observations and data presented here clearly indicate the physiological significance of lipid- and fatty acid-induced interfacial aggregation of Aβ, which could generate structurally and biologically unique oligomers that may be important in the AD pathology.

Conclusion -2: Prion Type Self-propagation: A Unique Property of 'Off-pathway' Oligomers

The prion-type *corruptive template-assisted* mechanism of infectivity is a newly emerging hypothesis among neurodegenerative diseases. Recent studies and finding have shown that synthetic as well as brain-derived Aβ can undergo prion type propagation and promote acceleration of disease in mouse models.[88, 89, 132] However, none of the reports demonstrate the molecular aspects of Aβ displaying prion characteristics. Previous studies have shown that *in vitro* Aβ oligomers like PFOs and FOs can display prion type behavior, but one important drawback of all these oligomers is that they are not biophysically well characterized, which is a limiting factor for understanding the details of the mechanism.[85, 86] One of the most significant findings of our studies is that we have shown that a unique, off-pathway, *in vitro* oligomer called LFAO, generated in the presence of fatty acid interfaces and biophysically well characterized, can undergo prion-type self propagation, quantitatively converting more monomers into toxic oligomers at the expense of fibrils.[113] Moreover, LFAOs can undergo similar *in vitro* amplification as has been shown for prions using the PMCA method.[112, 114] All these data and previous findings clearly indicate a common link between AD and prion toxicity mechanisms, which may be the underlying mechanism among many neurodegenerative disorders.

Future Work

Future studies will be directed towards elucidating the structure of LFAOs using biophysical techniques like Fourier transform infrared (FTIR) spectroscopy, mass spectrometry etc., which will provide a better understanding of their propagation mechanisms and help to further explore the similarities/dissimilarities between LFAOs and other known *in vitro* oligomers, on-pathway intermediates and fibrils.

The efficiency of LFAOs to cross seed and propagate other proteins will also be explored using similar experimental methodology as used for LFAO propagations. These proteins will include mutant forms of Aβ42 as well as both wild type and mutant forms of Aβ40 involved in both AD and cerebral amyloid angiopathy (CAA). In addition, cross seeding with Parkinson's-associated α-synuclein will be also investigated. This study will help to explore whether all these neurodegenerative disorders are interconnected and whether one can increase the chance of occurrence or severity for others.

Finally, toxicity of LFAOs will be explored on human neuroblastoma cells using the XTT reduction assay. Furthermore, we will also explore the effect of LFAOs on NF-κB activation, which is involved in Aβ-induced endothelial adhesion and transmigration.

REFERENCES

1. Binder, L. I.; Guillozet-Bongaarts, A. L.; Garcia-Sierra, F.; Berry, R. W. Tau, tangles, and Alzheimer's disease. *Biochim Biophys Acta* **2005,** *1739* (2-3), 216-23.

2. Selkoe, D. J.; Podlisny, M. B. Deciphering the genetic basis of Alzheimer's disease. *Annu Rev Genomics Hum Genet* **2002,** *3,* 67-99.

3. Golde, T. E. Alzheimer disease therapy: can the amyloid cascade be halted? *J Clin Invest* **2003,** *111* (1), 11-8.

4. Selkoe, D. J. Alzheimer's disease: genes, proteins, and therapy. *Physiol Rev* **2001,** *81* (2), 741-66.

5. Brookmeyer, R.; Gray, S.; Kawas, C. Projections of Alzheimer's disease in the United States and the public health impact of delaying disease onset. *Am J Public Health* **1998,** *88* (9), 1337-42.

6. Haass, C.; Selkoe, D. J. Soluble protein oligomers in neurodegeneration: lessons from the Alzheimer's amyloid beta-peptide. *Nat Rev Mol Cell Biol* **2007,** *8* (2), 101-12.

7. Miller, D. L.; Papayannopoulos, I. A.; Styles, J.; Bobin, S. A.; Lin, Y. Y.; Biemann, K.; Iqbal, K. Peptide compositions of the cerebrovascular and senile plaque core amyloid deposits of Alzheimer's disease. *Arch Biochem Biophys* **1993,** *301* (1), 41-52.

8. Selkoe, D. J. Deciphering Alzheimer's disease: the amyloid precursor protein yields new clues. *Science* **1990,** *248* (4959), 1058-60.

9. Vassar, R.; Bennett, B. D.; Babu-Khan, S.; Kahn, S.; Mendiaz, E. A.; Denis, P.; Teplow, D. B.; Ross, S.; Amarante, P.; Loeloff, R.; Luo, Y.; Fisher, S.; Fuller, J.; Edenson, S.; Lile, J.; Jarosinski, M. A.; Biere, A. L.; Curran, E.; Burgess, T.; Louis, J. C.;

Collins, F.; Treanor, J.; Rogers, G.; Citron, M. Beta-secretase cleavage of Alzheimer's amyloid precursor protein by the transmembrane aspartic protease BACE. *Science* **1999,** *286* (5440), 735-41.

10. Kimberly, W. T.; LaVoie, M. J.; Ostaszewski, B. L.; Ye, W.; Wolfe, M. S.; Selkoe, D. J. Gamma-secretase is a membrane protein complex comprised of presenilin, nicastrin, Aph-1, and Pen-2. *Proc Natl Acad Sci U S A* **2003,** *100* (11), 6382-7.

11. Harper, J. D.; Lansbury, P. T., Jr. Models of amyloid seeding in Alzheimer's disease and scrapie: mechanistic truths and physiological consequences of the time-dependent solubility of amyloid proteins. *Annu Rev Biochem* **1997,** *66*, 385-407.

12. Lomakin, A.; Teplow, D. B.; Kirschner, D. A.; Benedek, G. B. Kinetic theory of fibrillogenesis of amyloid beta-protein. *Proc Natl Acad Sci U S A* **1997,** *94* (15), 7942-7.

13. Walsh, D. M.; Lomakin, A.; Benedek, G. B.; Condron, M. M.; Teplow, D. B. Amyloid beta-protein fibrillogenesis. Detection of a protofibrillar intermediate. *J Biol Chem* **1997,** *272* (35), 22364-72.

14. Evans, K. C.; Berger, E. P.; Cho, C. G.; Weisgraber, K. H.; Lansbury, P. T., Jr. Apolipoprotein E is a kinetic but not a thermodynamic inhibitor of amyloid formation: implications for the pathogenesis and treatment of Alzheimer disease. *Proc Natl Acad Sci U S A* **1995,** *92* (3), 763-7.

15. Hardy, J. A.; Higgins, G. A. Alzheimer's disease: the amyloid cascade hypothesis. *Science* **1992,** *256* (5054), 184-5.

16. Kawabata, S.; Higgins, G. A.; Gordon, J. W. Amyloid plaques, neurofibrillary tangles and neuronal loss in brains of transgenic mice overexpressing a C-terminal fragment of human amyloid precursor protein. *Nature* **1992,** *356* (6366), 265.

17. Hsiao, K.; Chapman, P.; Nilsen, S.; Eckman, C.; Harigaya, Y.; Younkin, S.; Yang, F.; Cole, G. Correlative memory deficits, Abeta elevation, and amyloid plaques in transgenic mice. *Science* **1996,** *274* (5284), 99-102.

18. Kawarabayashi, T.; Shoji, M.; Younkin, L. H.; Wen-Lang, L.; Dickson, D. W.; Murakami, T.; Matsubara, E.; Abe, K.; Ashe, K. H.; Younkin, S. G. Dimeric amyloid beta protein rapidly accumulates in lipid rafts followed by apolipoprotein E and phosphorylated tau accumulation in the Tg2576 mouse model of Alzheimer's disease. *J Neurosci* **2004,** *24* (15), 3801-9.

19. McLean, C. A.; Cherny, R. A.; Fraser, F. W.; Fuller, S. J.; Smith, M. J.; Beyreuther, K.; Bush, A. I.; Masters, C. L. Soluble pool of Abeta amyloid as a determinant of severity of neurodegeneration in Alzheimer's disease. *Ann Neurol* **1999,** *46* (6), 860-6.

20. Townsend, M.; Shankar, G. M.; Mehta, T.; Walsh, D. M.; Selkoe, D. J. Effects of secreted oligomers of amyloid beta-protein on hippocampal synaptic plasticity: a potent role for trimers. *J Physiol* **2006,** *572* (Pt 2), 477-92.

21. Westerman, M. A.; Cooper-Blacketer, D.; Mariash, A.; Kotilinek, L.; Kawarabayashi, T.; Younkin, L. H.; Carlson, G. A.; Younkin, S. G.; Ashe, K. H. The relationship between Abeta and memory in the Tg2576 mouse model of Alzheimer's disease. *J Neurosci* **2002,** *22* (5), 1858-67.

22. Walsh, D. M.; Klyubin, I.; Fadeeva, J. V.; Rowan, M. J.; Selkoe, D. J. Amyloid-beta oligomers: their production, toxicity and therapeutic inhibition. *Biochem Soc Trans* **2002,** *30* (4), 552-7.

23. Blackley, H. K.; Sanders, G. H.; Davies, M. C.; Roberts, C. J.; Tendler, S. J.; Wilkinson, M. J. In-situ atomic force microscopy study of beta-amyloid fibrillization. *J Mol Biol* **2000,** *298* (5), 833-40.

24. Harper, J. D.; Wong, S. S.; Lieber, C. M.; Lansbury, P. T., Jr. Assembly of A beta amyloid protofibrils: an in vitro model for a possible early event in Alzheimer's disease. *Biochemistry* **1999,** *38* (28), 8972-80.

25. Ionescu-Zanetti, C.; Khurana, R.; Gillespie, J. R.; Petrick, J. S.; Trabachino, L. C.; Minert, L. J.; Carter, S. A.; Fink, A. L. Monitoring the assembly of Ig light-chain amyloid fibrils by atomic force microscopy. *Proc Natl Acad Sci U S A* **1999,** *96* (23), 13175-9.

26. Walsh, D. M.; Hartley, D. M.; Kusumoto, Y.; Fezoui, Y.; Condron, M. M.; Lomakin, A.; Benedek, G. B.; Selkoe, D. J.; Teplow, D. B. Amyloid beta-protein fibrillogenesis. Structure and biological activity of protofibrillar intermediates. *J Biol Chem* **1999,** *274* (36), 25945-52.

27. Ward, R. V.; Jennings, K. H.; Jepras, R.; Neville, W.; Owen, D. E.; Hawkins, J.; Christie, G.; Davis, J. B.; George, A.; Karran, E. H.; Howlett, D. R. Fractionation and characterization of oligomeric, protofibrillar and fibrillar forms of beta-amyloid peptide. *Biochem J* **2000,** *348 Pt 1*, 137-44.

28. Lesne, S.; Koh, M. T.; Kotilinek, L.; Kayed, R.; Glabe, C. G.; Yang, A.; Gallagher, M.; Ashe, K. H. A specific amyloid-beta protein assembly in the brain impairs memory. *Nature* **2006,** *440* (7082), 352-7.

29. Shankar, G. M.; Li, S.; Mehta, T. H.; Garcia-Munoz, A.; Shepardson, N. E.; Smith, I.; Brett, F. M.; Farrell, M. A.; Rowan, M. J.; Lemere, C. A.; Regan, C. M.; Walsh, D. M.; Sabatini, B. L.; Selkoe, D. J. Amyloid-beta protein dimers isolated directly

from Alzheimer's brains impair synaptic plasticity and memory. *Nat Med* **2008,** *14* (8), 837-42.

30. Walsh, D. M.; Klyubin, I.; Fadeeva, J. V.; Cullen, W. K.; Anwyl, R.; Wolfe, M. S.; Rowan, M. J.; Selkoe, D. J. Naturally secreted oligomers of amyloid beta protein potently inhibit hippocampal long-term potentiation in vivo. *Nature* **2002,** *416* (6880), 535-9.

31. Cleary, J. P.; Walsh, D. M.; Hofmeister, J. J.; Shankar, G. M.; Kuskowski, M. A.; Selkoe, D. J.; Ashe, K. H. Natural oligomers of the amyloid-beta protein specifically disrupt cognitive function. *Nat Neurosci* **2005,** *8* (1), 79-84.

32. Lacor, P. N.; Buniel, M. C.; Chang, L.; Fernandez, S. J.; Gong, Y.; Viola, K. L.; Lambert, M. P.; Velasco, P. T.; Bigio, E. H.; Finch, C. E.; Krafft, G. A.; Klein, W. L. Synaptic targeting by Alzheimer's-related amyloid beta oligomers. *J Neurosci* **2004,** *24* (45), 10191-200.

33. Podlisny, M. B.; Ostaszewski, B. L.; Squazzo, S. L.; Koo, E. H.; Rydell, R. E.; Teplow, D. B.; Selkoe, D. J. Aggregation of secreted amyloid beta-protein into sodium dodecyl sulfate-stable oligomers in cell culture. *J Biol Chem* **1995,** *270* (16), 9564-70.

34. Klyubin, I.; Walsh, D. M.; Lemere, C. A.; Cullen, W. K.; Shankar, G. M.; Betts, V.; Spooner, E. T.; Jiang, L.; Anwyl, R.; Selkoe, D. J.; Rowan, M. J. Amyloid beta protein immunotherapy neutralizes Abeta oligomers that disrupt synaptic plasticity in vivo. *Nat Med* **2005,** *11* (5), 556-61.

35. Walsh, D. M.; Townsend, M.; Podlisny, M. B.; Shankar, G. M.; Fadeeva, J. V.; El Agnaf, O.; Hartley, D. M.; Selkoe, D. J. Certain inhibitors of synthetic amyloid beta-

peptide (Abeta) fibrillogenesis block oligomerization of natural Abeta and thereby rescue long-term potentiation. *J Neurosci* **2005,** *25* (10), 2455-62.

36. Glabe, C. G. Structural classification of toxic amyloid oligomers. *J Biol Chem* **2008,** *283* (44), 29639-43.

37. Barghorn, S.; Nimmrich, V.; Striebinger, A.; Krantz, C.; Keller, P.; Janson, B.; Bahr, M.; Schmidt, M.; Bitner, R. S.; Harlan, J.; Barlow, E.; Ebert, U.; Hillen, H. Globular amyloid beta-peptide oligomer - a homogenous and stable neuropathological protein in Alzheimer's disease. *J Neurochem* **2005,** *95* (3), 834-47.

38. Lambert, M. P.; Barlow, A. K.; Chromy, B. A.; Edwards, C.; Freed, R.; Liosatos, M.; Morgan, T. E.; Rozovsky, I.; Trommer, B.; Viola, K. L.; Wals, P.; Zhang, C.; Finch, C. E.; Krafft, G. A.; Klein, W. L. Diffusible, nonfibrillar ligands derived from Abeta1-42 are potent central nervous system neurotoxins. *Proc Natl Acad Sci U S A* **1998,** *95* (11), 6448-53.

39. Selkoe, D. J. Soluble oligomers of the amyloid beta-protein impair synaptic plasticity and behavior. *Behav Brain Res* **2008,** *192* (1), 106-13.

40. Chromy, B. A.; Nowak, R. J.; Lambert, M. P.; Viola, K. L.; Chang, L.; Velasco, P. T.; Jones, B. W.; Fernandez, S. J.; Lacor, P. N.; Horowitz, P.; Finch, C. E.; Krafft, G. A.; Klein, W. L. Self-assembly of Abeta(1-42) into globular neurotoxins. *Biochemistry* **2003,** *42* (44), 12749-60.

41. Gellermann, G. P.; Byrnes, H.; Striebinger, A.; Ullrich, K.; Mueller, R.; Hillen, H.; Barghorn, S. Abeta-globulomers are formed independently of the fibril pathway. *Neurobiol Dis* **2008,** *30* (2), 212-20.

42. Goldsbury, C. S.; Wirtz, S.; Muller, S. A.; Sunderji, S.; Wicki, P.; Aebi, U.; Frey, P. Studies on the in vitro assembly of a beta 1-40: implications for the search for a beta fibril formation inhibitors. *J Struct Biol* **2000,** *130* (2-3), 217-31.

43. Chien, P.; Weissman, J. S.; DePace, A. H. Emerging principles of conformation-based prion inheritance. *Annu Rev Biochem* **2004,** *73*, 617-56.

44. Petkova, A. T.; Leapman, R. D.; Guo, Z.; Yau, W. M.; Mattson, M. P.; Tycko, R. Self-propagating, molecular-level polymorphism in Alzheimer's beta-amyloid fibrils. *Science* **2005,** *307* (5707), 262-5.

45. Tycko, R. Progress towards a molecular-level structural understanding of amyloid fibrils. *Curr Opin Struct Biol* **2004,** *14* (1), 96-103.

46. Necula, M.; Kayed, R.; Milton, S.; Glabe, C. G. Small molecule inhibitors of aggregation indicate that amyloid beta oligomerization and fibrillization pathways are independent and distinct. *J Biol Chem* **2007,** *282* (14), 10311-24.

47. Kayed, R.; Pensalfini, A.; Margol, L.; Sokolov, Y.; Sarsoza, F.; Head, E.; Hall, J.; Glabe, C. Annular protofibrils are a structurally and functionally distinct type of amyloid oligomer. *J Biol Chem* **2009,** *284* (7), 4230-7.

48. Lambert, M. P.; Velasco, P. T.; Chang, L.; Viola, K. L.; Fernandez, S.; Lacor, P. N.; Khuon, D.; Gong, Y.; Bigio, E. H.; Shaw, P.; De Felice, F. G.; Krafft, G. A.; Klein, W. L. Monoclonal antibodies that target pathological assemblies of Abeta. *J Neurochem* **2007,** *100* (1), 23-35.

49. Nimmrich, V.; Grimm, C.; Draguhn, A.; Barghorn, S.; Lehmann, A.; Schoemaker, H.; Hillen, H.; Gross, G.; Ebert, U.; Bruehl, C. Amyloid beta oligomers (A

beta(1-42) globulomer) suppress spontaneous synaptic activity by inhibition of P/Q-type calcium currents. *J Neurosci* **2008,** *28* (4), 788-97.

50. Pratt, L. R.; Pohorille, A. Hydrophobic effects and modeling of biophysical aqueous solution interfaces. *Chem Rev* **2002,** *102* (8), 2671-92.

51. Schladitz, C.; Vieira, E. P.; Hermel, H.; Mohwald, H. Amyloid-beta-sheet formation at the air-water interface. *Biophys J* **1999,** *77* (6), 3305-10.

52. Nichols, M. R.; Moss, M. A.; Reed, D. K.; Hoh, J. H.; Rosenberry, T. L. Amyloid-beta aggregates formed at polar-nonpolar interfaces differ from amyloid-beta protofibrils produced in aqueous buffers. *Microsc Res Tech* **2005,** *67* (3-4), 164-74.

53. Nichols, M. R.; Moss, M. A.; Reed, D. K.; Cratic-McDaniel, S.; Hoh, J. H.; Rosenberry, T. L. Amyloid-beta protofibrils differ from amyloid-beta aggregates induced in dilute hexafluoroisopropanol in stability and morphology. *J Biol Chem* **2005,** *280* (4), 2471-80.

54. Florent-Bechard, S.; Desbene, C.; Garcia, P.; Allouche, A.; Youssef, I.; Escanye, M. C.; Koziel, V.; Hanse, M.; Malaplate-Armand, C.; Stenger, C.; Kriem, B.; Yen-Potin, F. T.; Olivier, J. L.; Pillot, T.; Oster, T. The essential role of lipids in Alzheimer's disease. *Biochimie* **2009,** *91* (6), 804-9.

55. Simons, K.; Vaz, W. L. Model systems, lipid rafts, and cell membranes. *Annu Rev Biophys Biomol Struct* **2004,** *33*, 269-95.

56. Lee, S. J.; Liyanage, U.; Bickel, P. E.; Xia, W.; Lansbury, P. T., Jr.; Kosik, K. S. A detergent-insoluble membrane compartment contains A beta in vivo. *Nat Med* **1998,** *4* (6), 730-4.

57. Riddell, D. R.; Christie, G.; Hussain, I.; Dingwall, C. Compartmentalization of beta-secretase (Asp2) into low-buoyant density, noncaveolar lipid rafts. *Curr Biol* **2001,** *11* (16), 1288-93.

58. Wahrle, S.; Das, P.; Nyborg, A. C.; McLendon, C.; Shoji, M.; Kawarabayashi, T.; Younkin, L. H.; Younkin, S. G.; Golde, T. E. Cholesterol-dependent gamma-secretase activity in buoyant cholesterol-rich membrane microdomains. *Neurobiol Dis* **2002,** *9* (1), 11-23.

59. Knight, J. D.; Miranker, A. D. Phospholipid catalysis of diabetic amyloid assembly. *J Mol Biol* **2004,** *341* (5), 1175-87.

60. Zhang, Q.; Powers, E. T.; Nieva, J.; Huff, M. E.; Dendle, M. A.; Bieschke, J.; Glabe, C. G.; Eschenmoser, A.; Wentworth, P., Jr.; Lerner, R. A.; Kelly, J. W. Metabolite-initiated protein misfolding may trigger Alzheimer's disease. *Proc Natl Acad Sci U S A* **2004,** *101* (14), 4752-7.

61. Zhao, H.; Tuominen, E. K.; Kinnunen, P. K. Formation of amyloid fibers triggered by phosphatidylserine-containing membranes. *Biochemistry* **2004,** *43* (32), 10302-7.

62. Bokvist, M.; Lindstrom, F.; Watts, A.; Grobner, G. Two types of Alzheimer's beta-amyloid (1-40) peptide membrane interactions: aggregation preventing transmembrane anchoring versus accelerated surface fibril formation. *J Mol Biol* **2004,** *335* (4), 1039-49.

63. Irminger-Finger, I.; Siegel, B. D.; Leung, W. C. The functions of breast cancer susceptibility gene 1 (BRCA1) product and its associated proteins. *Biol Chem* **1999,** *380* (2), 117-28.

64. Martins, I. C.; Kuperstein, I.; Wilkinson, H.; Maes, E.; Vanbrabant, M.; Jonckheere, W.; Van Gelder, P.; Hartmann, D.; D'Hooge, R.; De Strooper, B.; Schymkowitz, J.; Rousseau, F. Lipids revert inert Abeta amyloid fibrils to neurotoxic protofibrils that affect learning in mice. *EMBO J* **2008,** *27* (1), 224-33.

65. McLaurin, J.; Franklin, T.; Fraser, P. E.; Chakrabartty, A. Structural transitions associated with the interaction of Alzheimer beta-amyloid peptides with gangliosides. *J Biol Chem* **1998,** *273* (8), 4506-15.

66. Rushworth, J. V.; Hooper, N. M. Lipid Rafts: Linking Alzheimer's Amyloid-beta Production, Aggregation, and Toxicity at Neuronal Membranes. *Int J Alzheimers Dis 2011*, 603052.

67. Choo-Smith, L. P.; Garzon-Rodriguez, W.; Glabe, C. G.; Surewicz, W. K. Acceleration of amyloid fibril formation by specific binding of Abeta-(1-40) peptide to ganglioside-containing membrane vesicles. *J Biol Chem* **1997,** *272* (37), 22987-90.

68. Choo-Smith, L. P.; Surewicz, W. K. The interaction between Alzheimer amyloid beta(1-40) peptide and ganglioside GM1-containing membranes. *FEBS Lett* **1997,** *402* (2-3), 95-8.

69. Kakio, A.; Nishimoto, S.; Yanagisawa, K.; Kozutsumi, Y.; Matsuzaki, K. Interactions of amyloid beta-protein with various gangliosides in raft-like membranes: importance of GM1 ganglioside-bound form as an endogenous seed for Alzheimer amyloid. *Biochemistry* **2002,** *41* (23), 7385-90.

70. Terzi, E.; Holzemann, G.; Seelig, J. Interaction of Alzheimer beta-amyloid peptide(1-40) with lipid membranes. *Biochemistry* **1997,** *36* (48), 14845-52.

71. Yip, C. M.; McLaurin, J. Amyloid-beta peptide assembly: a critical step in fibrillogenesis and membrane disruption. *Biophys J* **2001,** *80* (3), 1359-71.

72. Yamamoto, N.; Hasegawa, K.; Matsuzaki, K.; Naiki, H.; Yanagisawa, K. Environment- and mutation-dependent aggregation behavior of Alzheimer amyloid beta-protein. *J Neurochem* **2004,** *90* (1), 62-9.

73. Coles, M.; Bicknell, W.; Watson, A. A.; Fairlie, D. P.; Craik, D. J. Solution structure of amyloid beta-peptide(1-40) in a water-micelle environment. Is the membrane-spanning domain where we think it is? *Biochemistry* **1998,** *37* (31), 11064-77.

74. Shao, H.; Jao, S.; Ma, K.; Zagorski, M. G. Solution structures of micelle-bound amyloid beta-(1-40) and beta-(1-42) peptides of Alzheimer's disease. *J Mol Biol* **1999,** *285* (2), 755-73.

75. Rangachari, V.; Moore, B. D.; Reed, D. K.; Sonoda, L. K.; Bridges, A. W.; Conboy, E.; Hartigan, D.; Rosenberry, T. L. Amyloid-beta(1-42) rapidly forms protofibrils and oligomers by distinct pathways in low concentrations of sodium dodecylsulfate. *Biochemistry* **2007,** *46* (43), 12451-62.

76. Rangachari, V.; Reed, D. K.; Moore, B. D.; Rosenberry, T. L. Secondary structure and interfacial aggregation of amyloid-beta(1-40) on sodium dodecyl sulfate micelles. *Biochemistry* **2006,** *45* (28), 8639-48.

77. Prusiner, S. B. Prions. *Proc Natl Acad Sci U S A* **1998,** *95* (23), 13363-83.

78. Soto, C.; Castilla, J. The controversial protein-only hypothesis of prion propagation. *Nat Med* **2004,** *10 Suppl*, S63-7.

79. Griffith, J. S. Self-replication and scrapie. *Nature* **1967,** *215* (5105), 1043-4.

80. Desplats, P.; Lee, H. J.; Bae, E. J.; Patrick, C.; Rockenstein, E.; Crews, L.; Spencer, B.; Masliah, E.; Lee, S. J. Inclusion formation and neuronal cell death through neuron-to-neuron transmission of alpha-synuclein. *Proc Natl Acad Sci U S A* **2009,** *106* (31), 13010-5.

81. Hansen, C.; Angot, E.; Bergstrom, A. L.; Steiner, J. A.; Pieri, L.; Paul, G.; Outeiro, T. F.; Melki, R.; Kallunki, P.; Fog, K.; Li, J. Y.; Brundin, P. Alpha-Synuclein propagates from mouse brain to grafted dopaminergic neurons and seeds aggregation in cultured human cells. *J Clin Invest 121* (2), 715-25.

82. Chia, R.; Tattum, M. H.; Jones, S.; Collinge, J.; Fisher, E. M.; Jackson, G. S. Superoxide dismutase 1 and tgSOD1 mouse spinal cord seed fibrils, suggesting a propagative cell death mechanism in amyotrophic lateral sclerosis. *PLoS One 5* (5), e10627.

83. Furukawa, Y.; Kaneko, K.; Watanabe, S.; Yamanaka, K.; Nukina, N. A seeding reaction recapitulates intracellular formation of Sarkosyl-insoluble transactivation response element (TAR) DNA-binding protein-43 inclusions. *J Biol Chem 286* (21), 18664-72.

84. Munch, C.; O'Brien, J.; Bertolotti, A. Prion-like propagation of mutant superoxide dismutase-1 misfolding in neuronal cells. *Proc Natl Acad Sci U S A 108* (9), 3548-53.

85. Kayed, R.; Canto, I.; Breydo, L.; Rasool, S.; Lukacsovich, T.; Wu, J.; Albay, R., 3rd; Pensalfini, A.; Yeung, S.; Head, E.; Marsh, J. L.; Glabe, C. Conformation dependent monoclonal antibodies distinguish different replicating strains or conformers of prefibrillar Abeta oligomers. *Mol Neurodegener 5*, 57.

86. Wu, J. W.; Breydo, L.; Isas, J. M.; Lee, J.; Kuznetsov, Y. G.; Langen, R.; Glabe, C. Fibrillar oligomers nucleate the oligomerization of monomeric amyloid beta but do not seed fibril formation. *J Biol Chem 285* (9), 6071-9.

87. Meyer-Luehmann, M.; Coomaraswamy, J.; Bolmont, T.; Kaeser, S.; Schaefer, C.; Kilger, E.; Neuenschwander, A.; Abramowski, D.; Frey, P.; Jaton, A. L.; Vigouret, J. M.; Paganetti, P.; Walsh, D. M.; Mathews, P. M.; Ghiso, J.; Staufenbiel, M.; Walker, L. C.; Jucker, M. Exogenous induction of cerebral beta-amyloidogenesis is governed by agent and host. *Science* **2006,** *313* (5794), 1781-4.

88. Langer, F.; Eisele, Y. S.; Fritschi, S. K.; Staufenbiel, M.; Walker, L. C.; Jucker, M. Soluble Abeta seeds are potent inducers of cerebral beta-amyloid deposition. *J Neurosci 31* (41), 14488-95.

89. Stohr, J.; Watts, J. C.; Mensinger, Z. L.; Oehler, A.; Grillo, S. K.; DeArmond, S. J.; Prusiner, S. B.; Giles, K. Purified and synthetic Alzheimer's amyloid beta (Abeta) prions. *Proc Natl Acad Sci U S A 109* (27), 11025-30.

90. Kumar, A.; Rice, B. L.; Patel, P.; Paslay, L. C.; Singh, D.; Bienkiewicz, E. A.; Morgan, S. E.; Rangachari, V. Non-esterified Fatty Acids Generate Distinct Low-molecular Weight Amyloid-b (Ab42) Oligomers along pathway Different from Fibril Formation. *PLoS One* **2011,** *6* (4), e18759.

91. Nielsen, L.; Khurana, R.; Coats, A.; Frokjaer, S.; Brange, J.; Vyas, S.; Uversky, V. N.; Fink, A. L. Effect of environmental factors on the kinetics of insulin fibril formation: elucidation of the molecular mechanism. *Biochemistry* **2001,** *40* (20), 6036-46.

92. Kumar, A.; Bullard, R. L.; Patel, P.; Paslay, L. C.; Singh, D.; Bienkiewicz, E. A.; Morgan, S. E.; Rangachari, V. Non-esterified fatty acids generate distinct low-molecular weight amyloid-beta (Abeta42) oligomers along pathway different from fibril formation. *PLoS One 6* (4), e18759.

93. Nichols, M. R.; Moss, M. A.; Reed, D. K.; Hoh, J. H.; Rosenberry, T. L. Rapid assembly of amyloid-beta peptide at a liquid/liquid interface produces unstable beta-sheet fibers. *Biochemistry* **2005,** *44* (1), 165-73.

94. Philo, J. S. Improved methods for fitting sedimentation coefficient distributions derived by time-derivative techniques. *Anal Biochem* **2006,** *354* (2), 238-46.

95. Schuck, P. Sedimentation analysis of noninteracting and self-associating solutes using numerical solutions to the Lamm equation. *Biophys J* **1998,** *75* (3), 1503-12.

96. Kim, S. I.; Yi, J. S.; Ko, Y. G. Amyloid beta oligomerization is induced by brain lipid rafts. *J Cell Biochem* **2006,** *99* (3), 878-89.

97. Waschuk, S. A.; Elton, E. A.; Darabie, A. A.; Fraser, P. E.; McLaurin, J. A. Cellular membrane composition defines A beta-lipid interactions. *J Biol Chem* **2001,** *276* (36), 33561-8.

98. Chirita, C. N.; Necula, M.; Kuret, J. Anionic micelles and vesicles induce tau fibrillization in vitro. *J Biol Chem* **2003,** *278* (28), 25644-50.

99. O'Nuallain, B.; Williams, A. D.; Westermark, P.; Wetzel, R. Seeding specificity in amyloid growth induced by heterologous fibrils. *J Biol Chem* **2004,** *279* (17), 17490-9.

100. Hasegawa, K.; Yamaguchi, I.; Omata, S.; Gejyo, F.; Naiki, H. Interaction between A beta(1-42) and A beta(1-40) in Alzheimer's beta-amyloid fibril formation in vitro. *Biochemistry* **1999,** *38* (47), 15514-21.

101. Jarrett, J. T.; Lansbury, P. T., Jr. Seeding "one-dimensional crystallization" of amyloid: a pathogenic mechanism in Alzheimer's disease and scrapie? *Cell* **1993,** *73* (6), 1055-8.

102. Wood, S. J.; Maleeff, B.; Hart, T.; Wetzel, R. Physical, morphological and functional differences between ph 5.8 and 7.4 aggregates of the Alzheimer's amyloid peptide Abeta. *J Mol Biol* **1996,** *256* (5), 870-7.

103. Bateman, A.; Bennett, H. P. Granulins: the structure and function of an emerging family of growth factors. *J Endocrinol* **1998,** *158* (2), 145-51.

104. Shao, W.; Yu, Z.; Chiang, Y.; Yang, Y.; Chai, T.; Foltz, W.; Lu, H.; Fantus, I. G.; Jin, T. Curcumin prevents high fat diet induced insulin resistance and obesity via attenuating lipogenesis in liver and inflammatory pathway in adipocytes. *PLoS One 7* (1), e28784.

105. Ghosh, P.; Kumar, A.; Datta, B.; Rangachari, V. Dynamics of protofibril elongation and association involved in Abeta42 peptide aggregation in Alzheimer's disease. *BMC Bioinformatics 11 Suppl 6*, S24.

106. Nichols, M. R.; Moss, M. A.; Reed, D. K.; Lin, W. L.; Mukhopadhyay, R.; Hoh, J. H.; Rosenberry, T. L. Growth of beta-amyloid(1-40) protofibrils by monomer elongation and lateral association. Characterization of distinct products by light scattering and atomic force microscopy. *Biochemistry* **2002,** *41* (19), 6115-27.

107. Lebowitz, J.; Lewis, M. S.; Schuck, P. Modern analytical ultracentrifugation in protein science: a tutorial review. *Protein Sci* **2002,** *11* (9), 2067-79.

108. Freir, D. B.; Nicoll, A. J.; Klyubin, I.; Panico, S.; Mc Donald, J. M.; Risse, E.; Asante, E. A.; Farrow, M. A.; Sessions, R. B.; Saibil, H. R.; Clarke, A. R.; Rowan, M. J.;

Walsh, D. M.; Collinge, J. Interaction between prion protein and toxic amyloid beta assemblies can be therapeutically targeted at multiple sites. *Nat Commun 2*, 336.

109. Collins, S. R.; Douglass, A.; Vale, R. D.; Weissman, J. S. Mechanism of prion propagation: amyloid growth occurs by monomer addition. *PLoS Biol* **2004,** *2* (10), e321.

110. King, C. Y.; Diaz-Avalos, R. Protein-only transmission of three yeast prion strains. *Nature* **2004,** *428* (6980), 319-23.

111. Tanaka, M.; Chien, P.; Yonekura, K.; Weissman, J. S. Mechanism of cross-species prion transmission: an infectious conformation compatible with two highly divergent yeast prion proteins. *Cell* **2005,** *121* (1), 49-62.

112. Saborio, G. P.; Permanne, B.; Soto, C. Sensitive detection of pathological prion protein by cyclic amplification of protein misfolding. *Nature* **2001,** *411* (6839), 810-3.

113. Kumar, A.; Paslay, L. C.; Lyons, D.; Morgan, S. E.; Correia, J. J.; Rangachari, V. Specific soluble oligomers of amyloid-beta peptide undergo replication and form non-fibrillar aggregates in interfacial environments. *J Biol Chem 287* (25), 21253-64.

114. Soto, C.; Anderes, L.; Suardi, S.; Cardone, F.; Castilla, J.; Frossard, M. J.; Peano, S.; Saa, P.; Limido, L.; Carbonatto, M.; Ironside, J.; Torres, J. M.; Pocchiari, M.; Tagliavini, F. Pre-symptomatic detection of prions by cyclic amplification of protein misfolding. *FEBS Lett* **2005,** *579* (3), 638-42.

115. Castilla, J.; Saa, P.; Hetz, C.; Soto, C. In vitro generation of infectious scrapie prions. *Cell* **2005,** *121* (2), 195-206.

116. Soto, C.; Saborio, G. P. Prions: disease propagation and disease therapy by conformational transmission. *Trends Mol Med* **2001,** *7* (3), 109-14.

117. Caughey, B.; Kocisko, D. A.; Raymond, G. J.; Lansbury, P. T., Jr. Aggregates of scrapie-associated prion protein induce the cell-free conversion of protease-sensitive prion protein to the protease-resistant state. *Chem Biol* **1995,** *2* (12), 807-17.

118. Gursky, O.; Aleshkov, S. Temperature-dependent beta-sheet formation in beta-amyloid Abeta(1-40) peptide in water: uncoupling beta-structure folding from aggregation. *Biochim Biophys Acta* **2000,** *1476* (1), 93-102.

119. Gast, K.; Modler, A. J.; Damaschun, H.; Krober, R.; Lutsch, G.; Zirwer, D.; Golbik, R.; Damaschun, G. Effect of environmental conditions on aggregation and fibril formation of barstar. *Eur Biophys J* **2003,** *32* (8), 710-23.

120. Lomakin, A.; Chung, D. S.; Benedek, G. B.; Kirschner, D. A.; Teplow, D. B. On the nucleation and growth of amyloid beta-protein fibrils: detection of nuclei and quantitation of rate constants. *Proc Natl Acad Sci U S A* **1996,** *93* (3), 1125-9.

121. Walter, M. F.; Mason, P. E.; Mason, R. P. Alzheimer's disease amyloid beta peptide 25-35 inhibits lipid peroxidation as a result of its membrane interactions. *Biochem Biophys Res Commun* **1997,** *233* (3), 760-4.

122. Pillot, T.; Goethals, M.; Vanloo, B.; Talussot, C.; Brasseur, R.; Vandekerckhove, J.; Rosseneu, M.; Lins, L. Fusogenic properties of the C-terminal domain of the Alzheimer beta-amyloid peptide. *J Biol Chem* **1996,** *271* (46), 28757-65.

123. Terzi, E.; Holzemann, G.; Seelig, J. Self-association of beta-amyloid peptide (1-40) in solution and binding to lipid membranes. *J Mol Biol* **1995,** *252* (5), 633-42.

124. Yamamoto, N.; Igbabvoa, U.; Shimada, Y.; Ohno-Iwashita, Y.; Kobayashi, M.; Wood, W. G.; Fujita, S. C.; Yanagisawa, K. Accelerated Abeta aggregation in the

presence of GM1-ganglioside-accumulated synaptosomes of aged apoE4-knock-in mouse brain. *FEBS Lett* **2004,** *569* (1-3), 135-9.

125. Yanagisawa, K. GM1 ganglioside and the seeding of amyloid in Alzheimer's disease: endogenous seed for Alzheimer amyloid. *Neuroscientist* **2005,** *11* (3), 250-60.

126. Yanagisawa, K.; Ihara, Y. GM1 ganglioside-bound amyloid beta-protein in Alzheimer's disease brain. *Neurobiol Aging* **1998,** *19* (1 Suppl), S65-7.

127. Assayag, K.; Yakunin, E.; Loeb, V.; Selkoe, D. J.; Sharon, R. Polyunsaturated fatty acids induce alpha-synuclein-related pathogenic changes in neuronal cells. *Am J Pathol* **2007,** *171* (6), 2000-11.

128. Lucke, C.; Gantz, D. L.; Klimtchuk, E.; Hamilton, J. A. Interactions between fatty acids and alpha-synuclein. *J Lipid Res* **2006,** *47* (8), 1714-24.

129. Ryan, T. M.; Howlett, G. J.; Bailey, M. F. Fluorescence detection of a lipid-induced tetrameric intermediate in amyloid fibril formation by apolipoprotein C-II. *J Biol Chem* **2008,** *283* (50), 35118-28.

130. Wang, F.; Yang, F.; Hu, Y.; Wang, X.; Jin, C.; Ma, J. Lipid interaction converts prion protein to a PrPSc-like proteinase K-resistant conformation under physiological conditions. *Biochemistry* **2007,** *46* (23), 7045-53.

131. Wang, F.; Wang, X.; Yuan, C. G.; Ma, J. Generating a prion with bacterially expressed recombinant prion protein. *Science 327* (5969), 1132-5.

132. Jucker, M.; Walker, L. C. Pathogenic protein seeding in Alzheimer disease and other neurodegenerative disorders. *Ann Neurol 70* (4), 532-40.